



1 **Reprocessing of XBT profiles from the Ligurian and Tyrrhenian seas over the** 2 **time period 1999-2019 with full metadata upgrade**

3 Simona Simoncelli¹, Franco Reseghetti², Claudia Fratianni¹, Lijing Cheng^{3,4}, Giancarlo Raiteri²

4 ¹ Istituto Nazionale di Geofisica e Vulcanologia (INGV), Viale Berti Pichat 6/2, 40127 Bologna, Italy;

5 ² ENEA, S. Teresa Marine Research Centre, 19032 Pozzuolo di Lerici, Italy;

6 ³ International Center for Climate and Environment Sciences, Institute of Atmospheric Physics, Chinese
7 Academy of Sciences, Beijing, 100029, China;

8 ⁴ Center for Ocean Mega-Science, Chinese Academy of Sciences, Qingdao, 266071, China;

9 *Correspondence to:* Simona Simoncelli (simona.simoncelli@ingv.it)

10 **Abstract**

11 The advent of open science and the United Nations Decade of Ocean Science for Sustainable Development
12 are revolutionizing the ocean data sharing landscape for an efficient and transparent ocean information and
13 knowledge generation. This blue revolution raised awareness on the importance of metadata and community
14 standards to actionate interoperability of the digital assets (data and services) and guarantee that data driven
15 science preserve provenance, lineage and quality information for its replicability. Historical data are frequently
16 not compliant with these criteria, lacking metadata information that was not retained crucial at the time of the
17 data generation and further ingestion into marine data infrastructures. The present data review is an example
18 attempt to fill this gap through a thorough data reprocessing starting from the original raw data and operational
19 log sheets. The data gathered using XBT (eXpendable BathyThermograph) probes during several monitoring
20 activities in the Tyrrhenian and Ligurian Seas between 1999 and 2019 have been first formatted and
21 standardized according to the latest community best practices and all available metadata have been inserted,
22 including calibration information never applied. Secondly, a new automatic Quality Control (QC) procedure
23 has been developed and a new interpolation scheme applied. The reprocessed (REP) dataset has been compared
24 to the present data version, available from SeaDataNet data access portal through the saved query Url
25 [https://cdi.seadatanet.org/search/welcome.php?query=1866&query_code={4E510DE6-CB22-47D5-B221-](https://cdi.seadatanet.org/search/welcome.php?query=1866&query_code={4E510DE6-CB22-47D5-B221-7275100CAB7F})
26 [7275100CAB7F}](https://cdi.seadatanet.org/search/welcome.php?query=1866&query_code={4E510DE6-CB22-47D5-B221-7275100CAB7F}), processed according to the pioneering work of Manzella et al. (2003) conducted in the
27 framework of the EU Mediterranean Forecasting System Pilot Project (Pinardi et al., 2003). The maximum
28 discrepancy among the REP and SDN data versions resides always within the surface layer (REP profiles are
29 warmer than SDN ones) until 150 m depth, generally when the thermocline settles (from May to November).
30 The overall bias and root mean square difference are equal to 0.002 °C and 0.041 °C, respectively. Such
31 differences are mainly due to the new interpolation technique (Barker and McDougall, 2020), the lack of
32 filtering and the application of the calibration correction in the REP dataset.

33 The REP dataset (Reseghetti et al., 2023; https://doi.org/10.13127/rep_xbt_1999_2019) is available and
34 accessible through the INGV ERDDAP server (<http://oceanbo.ingv.it/erddap/index.html>), which allows
35 machine to machine data access in compliance with the FAIR (Findable, Interoperable, Accessible, Reusable)
36 principles (Wilkinson et al., 2016).



37 **1 Introduction**

38 The open science paradigm boosted the sharing of data through different pathways determining the generation
39 of different versions of the same datasets. This might depend on the timeliness of data delivery, either in Near
40 Real Time (NRT) or Delayed Mode (DM), the data center managing the dataset, the data assembly center or
41 the marine data infrastructure collating it. The awareness of the importance of a complete metadata description
42 is increasing among the scientific community since it allows interoperability, traceability of the data lifecycle,
43 transparency and replicability of the knowledge generation process. In particular, some key information is
44 crucial in climate science because it allows to re-analyze historical data, quantifying and reducing
45 uncertainties, which are used to derive accurate scientific knowledge (Simoncelli et al., 2022).

46 The data provider should define the overall quality assurance strategy along with the data lifecycle to guarantee
47 the availability of the best data product, which implies the possibility of reprocessing the dataset according to
48 the state-of-the-art Quality Control (QC) procedures and standards. Data driven research should use the most
49 extensive datasets with complete metadata information passed through a trustworthy QC procedure. These are
50 also basic requirements to guarantee data reusability once the data are made openly accessible. The complete
51 set of metadata assures transparency of the data provenance and avoids the circulation of multiple versions.

52 The integration in global databases of data not compliant with these principles emerged recently for
53 measurements gathered in the last century, when the importance of storing data with complete ancillary
54 information was not yet clear. A striking example is provided by the XBT (eXpendable BathyThermograph)
55 probes, the oceanographic instruments that recorded the largest number of temperature profiles in the ocean
56 from the 1970s to the 1990s (Meyssignac et al., 2019). The complete metadata information is crucial for quality
57 control, data reprocessing (Cheng et al., 2014; 2018; Goni et al., 2019) and integration with other data types
58 to estimate key ocean monitoring indicators, such as the trend of global ocean heat content (Cheng et al., 2020;
59 2021; 2022), one of the most important climate change indicators. According to the literature (Cheng et al.,
60 2016 and 2017; Parks et al., 2022), the crucial metadata information that must be associated with XBT data
61 includes probe type and manufacturer, fall rate equation, launch height, and recording system. This information
62 was not mandatory for the data ingestion in the main marine data infrastructure, thus most historical data miss
63 it. For example, 50% of XBT profiles in the World Ocean Database (WOD) have no information about
64 manufacturer or probe type, necessitating the application of intelligent metadata techniques to complement it
65 (Palmer et al., 2018; Leahy et al., 2018; Haddad et al., 2022).

66 This data review originated from the recognition that the present version of historical XBTs from the Ligurian
67 and Tyrrhenian Seas, available through some main marine data infrastructures, SeaDataNet
68 (<https://www.seadatanet.org/>), World Ocean Database ([https://www.ncei.noaa.gov/products/world-ocean-](https://www.ncei.noaa.gov/products/world-ocean-database)
69 [database](https://www.ncei.noaa.gov/products/world-ocean-database)), Copernicus Marine Service (CMS, <https://marine.copernicus.eu/>), might differ and have incomplete
70 metadata description. Our objective was to recover the raw data together with the full metadata description
71 and secure them to the future generation of scientists for their further use. This awareness raised contemporary
72 to the evolution of open science and FAIR (Findable, Accessible, Interoperable and Reusable) data
73 management principles, which motivated us to adopt the latest community standards, Quality Control (QC)



74 procedures, and to implement an ERDDAP server as data dissemination strategy. ERDDAP is an open source
75 environmental data server software developed by NOAA and used throughout the ocean observing community
76 (Pinaridi et al. 2019; Tanhua et al. 2019) which allows us to become a node of the present data digital ecosystem,
77 in line with one of the expected societal outcomes (“transparent and accessible” ocean) of the UN Decade of
78 Ocean Science 2021-2030 (Ryabinin et al., 2019; Simoncelli et al., 2022).

79 The paper describes the reprocessing of temperature profiles from expendable probes recorded between 1999
80 and 2019 in the Ligurian and Tyrrhenian seas, most of them from ro-pax (Roll-on/roll-off Passengers) vessels
81 operating between the Italian ports of Genova and Palermo within the Ships Of Opportunity Program (SOOP)
82 of the Global Ocean Observing System (GOOS), currently identified as MX04 line. Additional XBT data were
83 collected through ancillary monitoring surveys with commercial and research vessels. The dataset contains
84 some XCTD profiles (less than 1%) too. The reprocessed dataset (REP) is obtained from the original raw XBT
85 profiles (the readable output of the DAQs). A correction based on the DAQ calibration (when available) is
86 applied to each temperature recorded value but also provided as separate information, to allow the user to
87 eventually subtract it. Automated QC tests specifically tuned for western Mediterranean basins based on the
88 latest documented QC procedures and best practices to assign a Quality Flag are applied, followed by
89 interpolation of raw profiles at a 1 m in depth. All available information collected during data-taking has been
90 added in the metadata section, according to the SeaDataNet (SDN) standards
91 (<https://www.seadatanet.org/Standards>) and IQuOD (International Quality-controlled Ocean Database,
92 <https://www.iquod.org/index.html>) recommendations.

93 The REP data product allows the user to select from the original profiles to the validated and interpolated ones,
94 filtering on the basis of the required quality level, selecting the Quality Flags (QF) associated with both the
95 raw and the interpolated data. Furthermore, the dataset is accessible through the ERDDAP data server
96 (<http://oceanbo.ingv.it/erddap/index.html>) installed at INGV which provides a simple and consistent way to
97 download it in several common file formats.

98 This study was conducted in the framework of the MACMAP (Multidisciplinary Analysis of Climate change
99 indicators in the Mediterranean And Polar regions) project ([https://progetti.ingv.it/it/progetti-](https://progetti.ingv.it/it/progetti-dipartimentali/ambiente/macmap)
100 [dipartimentali/ambiente/macmap](https://progetti.ingv.it/it/progetti-dipartimentali/ambiente/macmap)) funded by INGV (<https://ror.org/00qps9a02>) (2020-2024) in technical
101 collaboration with ENEA and Grandi Navi Veloci (GNV) shipping company. In fact, the reprocessing of the
102 historical XBTs was preparatory to the automatic validation, management and publication of new XBT data
103 gathered on the MX04 line from September 2021, after two years interruption of the monitoring activity.

104 The paper is organized as follows: Section 2 describes the main characteristics of an XBT system; Section 3
105 describes the original dataset and the monitoring activities that sustained it; Section 4 describes the
106 methodology applied for the automatic QC and the correction derived from calibration; Section 5 is about the
107 results; Section 6 summarizes the main results and draws conclusions; Section 7 describes the REP dataset
108 findability and accessibility.



109 **2 The XBT system, its accuracy, resolution and uncertainties**

110 In the early 1960s American engineers, who thereafter founded the Sippican Co. (now part of the Lockheed
111 Martin Co., hereinafter Sippican), developed the first version of today's XBT probes following to a US Navy
112 call for a seawater temperature (T) profiler for military applications. Within a few years Sippican optimized
113 the original probe and marketed different XBT types with specifications suitable for variable depths and ship
114 speed. XBTs became very popular within the oceanographic community (Flierl and Robinson, 1977) allowing
115 the gathering of T profiles through the use of commercial vessels and not just research vessels.

116 The XBT system consists of: an expendable ballistic probe falling into seawater; a device (DAQ) that records
117 an electrical signal and converts it into usable numerical data (in combination with a computer unit) and the
118 connection between the falling probe and the DAQ (e.g. Goni et al., 2019 and Parks et al., 2022). The sensing
119 component is an NTC thermistor (mounted inside the ballistic probe), that changes its resistance according to
120 seawater T flowing through the central hole of the probe zinc nose where it is located. Its thermal time constant
121 τ (time needed to detect 63% of a thermal step signal) is in the range 0.080 - 0.130 s (so that five-tau rule
122 indicates a time of about 0.5 s to almost fully detect a step temperature change). Technical characteristics
123 required by Sippican for the used NTC thermistor (whose features and performances remained unchanged
124 since the early 1960s) put limits on high accuracy measurements with XBT probes.

125 Another essential component is the thin double copper wire which is part of the acquisition circuit and which
126 is unwound by two spools simultaneously (clockwise in the ship and counterclockwise in the falling probe), a
127 technique which decouples the XBT vertical falling motion through the seawater from the translational motion
128 of the ship. The non-uniform application of the insulating substance on the wire and its defective winding on
129 one of the spools are the cause of a significant part of faulty or prematurely interrupted acquisitions.

130 XBT probes do not house any pressure sensor and the depth associated with a temperature measurement is not
131 measured directly but estimated by a phenomenological Fall Rate Equation (FRE) provided by the
132 manufacturer with coefficients that depend on the probe type and which are valid for the world ocean. The
133 software transforms a time series of resistance values provided by the DAQ into a series of depth - T values
134 using first a resistance-to-temperature conversion relationship (identical for all XBT types because it is specific
135 for the thermistor used, see Appendix A) and thus applying the coefficients of a FRE specific to each probe.
136 Sippican has preset conservative values for the recording time in its acquisition software but these values can
137 be freely modified in order to use all the wire wound on the probe spools. The first column of Table 1 shows
138 the nominal values and the maximum recorded depth in the same areas for each specific probe type.

139 Each component of an XBT system contributes to the overall measurement accuracy on depth and T values.
140 According to Anderson (1980): “*Sippican specifies the system with a stated worst case temperature accuracy*
141 *± 0.2 °C (± 0.1 °C for the probe and ± 0.1 °C for a properly maintained and calibrated recorder... and depth*
142 *accuracy at ± 15 feet (4.6 m) or $\pm 2\%$, whichever is larger”. Recently the IQuOD group (Cowley et al., 2021)
143 released a summary of uncertainties on T and depth values of different oceanographic devices, and the reported
144 value for XBTs is in the range 0.1-0.2 °C and slightly depending on the manufacturer and the manufacturing
145 date.*



146 In Bordone et al. (2020) it was found that the XBT measurements in the Mediterranean below 100 m compared
147 to those of almost contemporaneous and co-located Argo profilers (in order to have a practically unchanged
148 measurand) are warmer by about 0.05 °C and with a value of 0.10°C as the standard uncertainty of XBT
149 measurements after correction obtained by comparing them with Argo profiles and which was later used in the
150 QC as the SD for the XBT values.

151 The first part of the XBT fall is critical and hard to describe: a probe needs a few seconds from when it hits
152 the sea surface to make its motion stable (a few tens of meters, given its falling speed of about 6 ms⁻¹, Bringas
153 and Goni, 2015). For this reason, careful data validation in the near surface layer and where the seasonal
154 thermocline occurs (i.e. depths shallower than 100 m in the analyzed basin of the Mediterranean Sea), is
155 crucial. Below the thermocline, or in the surface layer in the cold periods (due to homogeneous temperature
156 values), the nominal poor depth accuracy for XBT data does not affect the whole quality too much.

157 The depth resolution depends both on DAQ sampling rate and FRE of the XBT probe. All DAQ models used
158 in this dataset work at 10 Hz (i.e. a sample every 0.1 s, a time interval nearly coincident with the time constant
159 of the NTC thermistor) so that the depth resolution depends on specific FRE with actual values close to 0.6 m.
160 The T reading resolution is usually 0.01 °C when using the standard Sippican software while 0.001 °C is the
161 standard output for Devil/Quoll DAQs and some old Sippican software versions. Throughout the work, three
162 decimal digits are always used for T values (both raw and interpolated) and the derived quantities (i.e. vertical
163 gradient). The computer clock (always updated to the UTC value shortly before the start/after the end of
164 operations) provides the time coordinate of each profile. The differences recorded with respect to the standard
165 UTC time have always been close to 1 s, which corresponds to the instrument sensitivity, in a time interval of
166 one day.

167 Sippican's manuals released over the years (e.g. Sippican 1968, 1980, 1991, 2006, 2010 and 2014) and reports
168 (e.g. Sy, 1991; Cook and Sy, 2001; Sy and Wright, 2001; Parks et al., 2022) well describe the best practices
169 for XBT use. The checking of the XBT system with a test canister before and after data collection as well as
170 the complete description of the system characteristics in the metadata is binding for subsequent optimal use of
171 the measurements. The evaluation of the performances of the XBT system during data collection is a needed
172 step to improve the quality. When strip chart recorders were used, a preliminary and accurate calibration of
173 the acquisition unit with a test canister (an integral component of an XBT system, tester hereafter) was
174 mandatory (e.g. Sippican, 1968 and 1980; Plessey-Sippican, 1975) but this good practice has been frequently
175 disregarded over the years. This operational procedure has been applied only since July 2010 to the monitoring
176 activity along the MX04 line and to few other subsets of profiles. Based on the improvements described by
177 Reseghetti et al. (2018), a specific correction has been developed and is a key component of the information
178 never used in previous data versions and unlocked in the REP dataset (section 4.3)

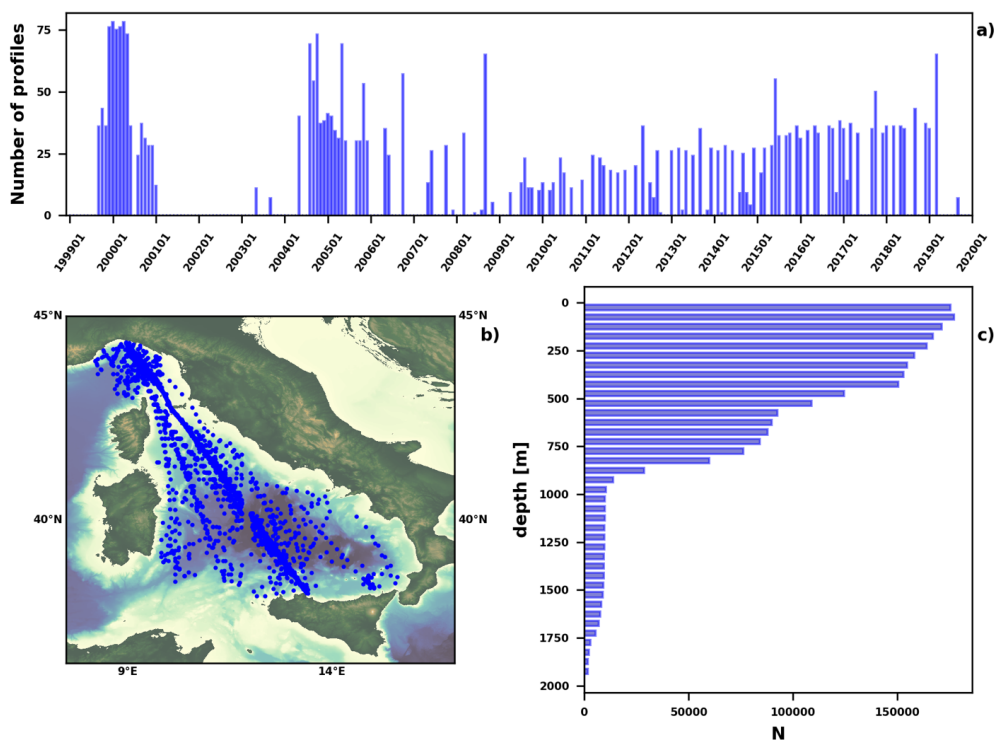
179 As for the XCTD-1 probes, there are some differences compared to the XBTs in terms of resolution and
180 accuracy, and a completely different recording circuitry. The manufacturer (the Japanese company TSK)
181 claims an accuracy of 0.02 °C on temperature (a factor of five better than XBTs) and a resolution of 0.01 °C
182 while the estimated uncertainty on the depth is the same as for the XBT probes (i.e. 4.6 m or 2%, whichever



183 is greater). The sampling frequency is 25 Hz (i.e. a reading of the thermistor resistance value every 0.04 s),
184 and, thanks to a falling speed which is just over half that of the XBT probes, the depth resolution for the model
185 XCTD-1 is of about 0.14 m.

186 3 The dataset

187 3757 temperature profiles, collected from September 1999 to September 2019 in operations managed by
188 ENEA (S. Teresa Marine Research Centre, STE thereafter) mainly through the use of commercial ships, are
189 included in the REP dataset. They come from XBT probes, plus a few dozen of XCTDs. Figure 1 shows the
190 XBT profiles temporal and spatial distribution, highlighting their sparseness, mainly influenced by the
191 irregular monitoring activity and data concentration along the MX04 Genova-Palermo line. The vertical data
192 distribution (Figure 1c) is also non-homogeneous due to the local bathymetry, the use of different probe types
193 and the ship speed, which may affect the duration of the data acquisition.



194

195 **Figure 1 (a) temporal distribution of the REP (reprocessed) XBT profiles; (b) geographical location; (c) vertical**
196 **distribution in layers of 50 m of depth.**

197 Table 1 shows some of the characteristics of the expendable probes used in this dataset, the FRE coefficients
198 applied to calculate the depth and the weight of the various components of each probe (ZAMAK nose, body
199 and spool in plastic and copper wire, including the total quantity that can unwind from the on-board spool) in
200 order to evaluate the overall quantity of material abandoned at sea caused by the launch of these probes. We



201 have no information regarding the various components of the XCTD-1 probes but their nose is made of plastic
 202 material. Sippican is the manufacturer of all the used XBT probes as well as the XCTD-1 probes are
 203 manufactured by TSK - Tsurumi Seiki Co. and marketed in Italy by Sippican.

204 The profiles were gathered during the following monitoring activities:

- 205 1. SOOP monitoring on the Genova-Palermo MX04 line, which provides the greatest contribution both
 206 in terms of campaigns (1999-2000, 2004-2006, 2010-2019) and quantity of profiles;
- 207 2. SOOP monitoring in collaboration with CSIRO (an Australian Government Agency), from 2007 to
 208 2011;
- 209 3. Sporadic additional SOOP monitoring by ENEA-STE in the Mediterranean (2012-2014);
- 210 4. An agreement between ENEA and IIM (Italian Hydrographic Institute of the Navy), (2006 - 2019);
- 211 5. An operational collaboration between ENEA-STE and CNR-ISMAR (Lerici), (2000 - 2017).

212 The main characteristics of the vessels and the instrumentation used for the data collection are summarized in
 213 Appendix B.

214 **Table 1 Characteristics of the different probes used: nominal depth suggested (and guaranteed) by Sippican and**
 215 **experienced maximum depth in the Mediterranean; maximum ship speed suggested by Sippican for an optimal**
 216 **drop; coefficients of Fall Rate Equation $D(t) = At - Bt^2$ used for depth calculation (provided by the manufacturer**
 217 **or by IGOSS, Hanawa et al., 1995); amount of ZAMAK, copper and plastic for each probe type; number of probes**
 218 **originally considered and those actually included in the dataset.**

Probe type	Rated depth (max depth) (m)	Maximum ship speed (knots)	Coeff. A (ms ⁻¹)	Coeff. B (ms ⁻²)	ZAMAK (kg) ± 0.001	Plastic (kg) ± 0.001	Copper (kg) ± 0.002	Original no. profiles	REP dataset
T4	460 (583)	30	6.691	0.00225	0.613	0.052	0.202	1486	1426
T5	1830 (2272)	6	6.828	0.00182	0.613	0.125	0.357	61	61
T5/20	1830 (2248)	20	6.828	0.00182	0.613	0.125	0.726	197	187
T6	460 (588)	15	6.691	0.00225	0.613	0.052	0.158	69	69
T7	760 (977)	15	6.691	0.00225	0.576	0.052	0.240	66	60
DB	760 (962)	20	6.691	0.00225	0.576	0.052	0.294	1828	1747
T10	200 (292)	10	6.301	0.00216	0.613	0.052	0.098	175	172
XCTD-1	1100 (1100)	12	3.425432	0.00047	None	NA	0.440	35	35

219
 220 The first SOOP in the Mediterranean Sea (September 1999 - December 2000) started in the framework of the
 221 European Mediterranean Forecasting System Pilot Project (MFSPP, Pinardi et al., 2003; Manzella et al., 2003;
 222 Pinardi and Coppini, 2010) under INGV coordination to support the development of operational oceanography
 223 forecasting activities through the NRT provision of ocean observations. XBT profiles were collected along
 224 transects crossing the Mediterranean Sea designed to monitor the variability of the main circulation features



225 (e.g. Fusco et al., 2003; Zodiatis et al., 2005; Millot and Taupier-Letage, 2005a and 2005b). The MX04 line is
226 the only line still active on seasonal basis, thanks to the MACMAP project, using GNV ro-pax (Roll-on/roll-
227 off Passengers) ferries which connect daily (just under 20 hours sailing at about 22 knots) Genova (44.40 °N,
228 8.91 °E) to Palermo (38.13 °N, 13.36 °E).

229 Starting from September 1999, 20 campaigns were carried out, in collaboration between CNR-ISMAR and
230 ENEA-STE, with initial monthly monitoring frequency, then every 15 days (December 1999 - May 2000), and
231 again monthly frequency until December 2000. T4 probes (with some T6 probes) were launched at fixed
232 intervals of time (every 30 minutes), corresponding to a sampling distance of about 11 nm. A Sippican MK12
233 card inserted into the motherboard of a desktop running Windows 98 IIE and with the software set to stop
234 acquisition at 460 m depth was used. All the campaigns were carried out using the MV "Excelsior", its route
235 was always the same and almost coincident with track 44 of the altimetric satellites (Vignudelli et al., 2003).
236 After a hiatus of more than 3 years and a campaign in May 2004 to check slightly different operational
237 procedures, monitoring along the MX04 line resumed on a monthly basis from September 2004 to December
238 2005 (July and August excluded), with two additional cruises in May and October 2006, for a total of 17
239 campaigns within the EU MFS-Toward Environmental Prediction project (MFS-TEP, Manzella et al. 2007;
240 Pinardi and Coppini, 2010). The ships (always GNV vessels) followed a route with marginal differences
241 compared to the previous one due to the introduction of nature conservation limitations in the Tuscan
242 archipelago. In November 2004, February and December 2005 the route was significantly different due to bad
243 weather and sea conditions. The campaigns were planned to travel as close as possible to the passage date of
244 the Jason-1 altimetric satellite along track 44. T4 and DB XBT probes were usually deployed (with a few
245 XCTD-1 and some T6) and the sampling distance was variable from 8 to 12 nm. After a few months, the DAQ
246 (a Sippican MK21 ISA) showed a small degradation and an evident "noise" appeared in the recorded profiles
247 even with excellent operating conditions. Unlike MFS-PP, the acquisition software was set to use all the wire
248 available on the probe spool (i.e. 600 m for T4 and 1000 m for DB probes).

249 Monitoring on MX04 resumed in July 2010, managed directly by ENEA-STE and until January 2013 was
250 widely variable both in terms of frequency and sampling distance (due to the uncertainty in the supply of XBT
251 probes). A regular sampling scheme was then adopted with a launch every 10' of latitude (corresponding to
252 11-12 nm depending on the ship's course), excluding the archipelago of Toscana, with five to six annual
253 repetitions, following the same path as in 2004-2006 (excluding February 2013 and April 2014 because of bad
254 weather and sea conditions). From June 2015, the ships moved to a more westerly route in the northern part of
255 the transect crossing the Corsica Channel (this allows monitoring of the water exchange between the
256 Tyrrhenian Sea and the Ligurian Sea) to rejoin the previous one around at latitude 39°N. The number of drops
257 at fixed positions increased to thirty-seven, mainly DB probes while other XBT types were used in particular
258 areas due to the reduced bathymetry (T10) or with interesting deep thermal structures (T5/20).

259 A short SOOP activity in collaboration with CSIRO was completed between December 2007 and March 2011
260 (19 campaigns) using containerships from Hapag Lloyd (namely "Canberra Express", "Stadt Weimar" and
261 "Wellington Express") and CMA CGM ("CMA CGM Charcot") shipping companies, operating between



262 Northern European ports and Australia. These campaigns were characterized by irregular frequency
263 throughout the year, a very high launching platform (at least 25 m over the sea level or more) and a sampling
264 distance between 20 and 35 nm. XBT launches began near the Egadi Islands (west of Sicilia) and terminated
265 in the Corsica Channel, following a path halfway between the MX04 transect and the island of Sardegna.
266 CSIRO installed a Turo Devil DAQ on each vessel while ENEA-STE only provided the DB probes.
267 Some additional XBT profiles (mainly DB type) were gathered in the Ligurian Sea between May 2012 and
268 March 2014 on board the GNV ship "Excellent" (in 5 campaigns) and in 2014 two different cruises using a
269 Sippican MK21 USB onboard the container ship "Daniel A" from the Turkish shipping company ARKAS.
270 From 2006 to 2019, 10 campaigns were carried out in collaboration between ENEA and IIM, using the ships
271 "Ammiraglio Magnaghi", "Aretusa" and "Galatea", collecting a total of about 200 profiles using different XBT
272 types, deployed from different heights and using different DAQs.
273 Finally, an operational collaboration between ENEA-STE and CNR-ISMAR allowed to carry out 29
274 campaigns between 2000 and 2017 using vessels managed by the CNR (mainly RV "Urania", but also RV
275 "Minerva Uno" and "Ibis"), gathering several hundred profiles with different XBT probe types deployed from
276 different heights and recorded using four different Sippican DAQ units.

277 **4 Methodology**

278 Specific QC procedures for XBT profiles in the Mediterranean Sea were first developed by Manzella et al.
279 (2003) within the MFS-PP project and later improved in Manzella et al. (2007). Temperature observations in
280 the Mediterranean Sea, due to its thermohaline circulation, water masses characteristics and large temperature
281 variability, might present peculiar features like thermal inversions or zero thermal gradient in areas of deep
282 water formation, thus necessitating regional tuning of QC tests. The prior QC procedures included: detection
283 of profile's end, gross range check, position control, elimination of spikes, interpolation at 1 m intervals,
284 Gaussian smoothing, general malfunctioning control, comparison with climatology and final visual check by
285 operator. Some additional constraints were applied: elimination of the initial part of each profile (the first
286 acceptable value is at 4 m depth, following the standard international procedure), allowed temperature values
287 within the 10-30 °C interval, maximum temperature inversion of 4.5 °C in the 0-200 m layer, 1.5 °C below
288 200 m, and 3 °Cm⁻¹ as maximum thermal gradient. This QC has not been applied to the data released in NRT
289 through the GTS (Global Telecommunication System, <https://community.wmo.int/en/activity-areas/global-telecommunication-system-gts>) but only to the data made available in DM through the SDN infrastructure
290 (available through the relative saved query from the SDN CDI data access portal at
291 https://cdi.seadatanet.org/search/welcome.php?query=1866&query_code={4E510DE6-CB22-47D5-B221-7275100CAB7F}). The raw data for the GTS dissemination were provided to NOAA and in the early 2000s
292 the profiles were also heavily sub-sampled due to the low bit rate satellite system provided by Argos, the basic
293 GTS data transmission system (Manzella et al., 2003). These different dissemination channels contributed to
294 the existence of several versions of the same profile in different blue data infrastructures (i.e. WOD, SDN).
295
296



297 A new automated QC procedure, written in Python and structured as a package, has been implemented in the
298 framework of the MACMAP project starting from the original raw XBT profiles, considering the scientific
299 progress made in the field in the last two decades and the full metadata information available. The aim was
300 twofold: first to secure the best version and most complete dataset for further use to the scientific community;
301 secondly to implement an automated QC workflow for the seasonal XBT campaigns started in September 2021
302 thanks to the MACMAP project. This also allowed to refine and standardize the quality assurance procedures
303 on board of the vessels to record all ancillary information in a pre-defined format and minimize the impact of
304 different operators on the data quality. The calibration correction, detailed in section 4.3, has been added, when
305 available, to the raw data before the QC analysis. However it is provided as a separate variable associated with
306 each XBT profile and the user can eventually remove it. None of the original profiles has been eliminated but
307 integrated with quality indexes, with the exception of those repeated during data taking and those less than 50
308 m deep due to problems during acquisition. A final visual check has also been performed using ODV software
309 (R. Schlitzer, Ocean Data View, <https://odv.awi.de/>, 2023) which highlighted the presence of anomalous
310 behavior in some T profiles that the implemented automatic QC tests could not detect. Some examples will be
311 discussed in Section 5 (Figure 10). The REP dataset has been written in ODV format and imported as ODV
312 collection, which contains interpolated temperature profiles and corresponding quality flags of each profile,
313 together with spatio-temporal details, profile name and ship name. This visual check suggested assigning to
314 each profile a general QF, choosing between these two options: 1) *excellent* indicating all QC done and 2)
315 *mixed* indicating some problems, with comments to warn the user about the anomalous features.

316 **4.1 Basic automated Quality Control procedure**

317 The XBT raw profiles have been QCed using a sequence of independent tests, checking for invalid information
318 on geographic characteristics and for known signatures of spurious measurements. Results of each test are
319 recorded by inserting the relative flag to the corresponding measurement according to the scheme shown in
320 Table 2, while Figure 2 provides an example of the QC tests applied to a profile.

321 The independent QC tests are described hereafter.

322 **Position on land check**

323 The profile position should be located at sea, thus latitude and longitude of each profile is checked against
324 gridded GEBCO bathymetry (GEBCO Compilation Group, 2022) on a 15 arc-second interval grid to determine
325 if it is located on land or not: if the “height” is negative it is lower than sea level, and it is flagged as GOOD,
326 otherwise is flagged as BAD.

327 **Depth check**

328 The depth values of each XBT profile are compared to the *last good depth* value provided by the operator.
329 Depth values are flagged as GOOD if they are shallower than it otherwise they are flagged as BAD. The
330 corresponding local bottom depth extracted from GEBCO and the nominal rated depth by the manufacturer
331 are not used but annotated in the metadata to facilitate further analysis by expert users.



332 **Table 2 Summary of the automated QC tests and the assigned exit values to each measurement within a profile.**

Test #	Check	Description	Exit value	Exit value description
1	Position control	Function to detect incorrect longitude and latitude values	49/52	49 profile is at sea; 52 profile is on land.
2	Depth	Function to detect depth values out of extreme depths. The reference depth is the depth indicated by the operator.	49/52	49 depth is below reference depth values; 52 depth is above reference depth values
3	Gross range check	Function to detect T values out of ranges in Table 3	49/52	49: T inside the range 52: T is out of range
4	Surface	Function to flag the first 4 meters considering as reference std=0.1 and its growing	49-52	49: Good 50: Probably Good 51: Probably bad 52: Bad
5	vertical gradient	Function to detect stuck values, decreasing and increasing values according to gradient value and considering only the values that passed the previous checks	56-58	56: stuck value 57: negative gradient out of threshold 57#: negative gradient out of threshold in successive iteration (#) 58: positive gradient out of threshold 58#: positive gradient out of threshold in successive iteration (#)
6	wire break/stretch	Function based on vertical gradient check to identify wire break on shipside or on probe-side	61	61: wire break/stretch
7	Spike detection	Function to detect spike considering the median, media and thresholds s_k in Table 4	59	59: spike if $ T3 - \text{median}(T1, T2, T3, T4, T5) \neq 0$ and $ T3 - \text{mean}(T1, T2, T3, T4, T5) > s_k$
8	High Frequency spiking	Function to identify feature in the profile like critical drops	60	60: critical drop

333

334 **Gross range check**

335 It applies a gross filter on observed temperature considering T thresholds that vary on 5 vertical layers, as
 336 reported in Table 3. T thresholds have been defined analyzing the seasonal T distribution in 4 sub-regions
 337 displayed in Figure 3: 1) the Ligurian Sea; 2) the Northern Tyrrhenian Sea; 3) the South-West Tyrrhenian Sea;
 338 4) the South-East Tyrrhenian Sea. The domain subdivision is based on the mean circulation features at 15 m
 339 and 350 m depth, computed from the Mediterranean Sea reanalysis (Simoncelli et al., 2014) data over the time
 340 period 1999-2018 (Figure 3). A detailed description of the circulation is out of scope here but its main features
 341 are detailed in Pinardi et al. (2015) and von Schuckmann et al. (2016, section 3.1).

342 **Surface check**

343 The XBT measurements close to the sea surface are usually considered unreliable and thus excluded from
 344 further analysis (e.g. Bailey et al., 1994; Cowley and Krummel, 2022), due to reaching stability in motion and
 345 thermal adaptation to the surrounding environment. It is preferred that the user is provided all the original
 346 measurements by adding a test that analyzes the measurements in the surface layer and annotating the resulting
 347 quality information in the ancillary variables or quality flags. The proposed test chooses as reference the value
 348 recorded at time $t = 0.6$ s (the first value currently considered acceptable), calculates the differences between
 349 this value and shallower measurements and classifies them using the standard uncertainty on temperature
 350 attributable to an XBT probe (0.10 °C) as a metric. In detail, the temperature differences $T(t_{0.6}) - T(t_i)$, with $(0.0$
 351 $\leq t_i \leq 0.5)$ s are calculated and the QF is assigned as follows:



- 352 • GOOD if $|T(t0.6)-T(t_i)| \leq 1*\text{std}$;
- 353 • PROBABLY GOOD if $1*\text{std} < |T(t0.6)-T(t_i)| \leq 2*\text{std}$;
- 354 • PROBABLY BAD if $2*\text{std} < |T(t0.6)-T(t_i)| \leq 3*\text{std}$;
- 355 • BAD if $|T(t0.6)-T(t_i)| > 3*\text{std}$.

356 The flag GOOD means a value indistinguishable from the record at $t = 0.6$ s while PROBABLY GOOD defines
357 an excellent compatibility. The PROBABLY BAD and BAD flags simply indicate a difference greater than
358 the established threshold with respect to the reference value at $t = 0.6$ s.

359 Inversion and gradient checks

360 This test is performed to detect unrealistic T oscillations with abrupt T reversals or unusually large T gradients.
361 The vertical gradient is defined as the difference between vertically adjacent measurements, $T_z=(T_2-T_1)/(Z_2-$
362 $Z_1)$, where T_2 and T_1 are temperatures at depths Z_2 and Z_1 , with level 2 being deeper than level 1. This test is
363 applied three times iteratively discarding values that failed the test in the next iteration. The acceptable T
364 gradient ranges (Table 3) have been defined through a statistical analysis in 5 vertical layers and 4 sub-regions
365 (Figure 3) through an approach that blends expert decisions with statistical support. Due to the spatial
366 (horizontal and vertical) and temporal sparseness of the data, the 0.01% and 99.99% quantiles have been
367 computed in the 5 layers considering: 1) the whole dataset; 2) the 4 sub regions; 3) the entire domain but for 4
368 seasons. The thresholds are the absolute minimum 0.01% quantile and maximum 99.99% quantile deriving
369 from the three cases. The thresholds of the two deepest levels are from case 1, the upper layer uses values from
370 case 2 and the second and third layers use the results of case 3.

371 **Table 3 Temperature and thermal gradient thresholds defined in 5 layers.**

Layer	Temperature (°C)		Vertical Gradient (°Cm ⁻¹)	
0-100 m	12.000	30.000	-3.400	0.613
100-250 m	12.500	17.900	-0.317	0.244
250-450 m	12.700	15.500	-0.156	0.170
450-1000 m	13.100	14.800	-0.133	0.137
1000-2300 m	13.100	14.000	-0.094	0.090

372

373 Wire break/stretch

374 Results of inversion and gradient checks are used to identify sharp variations toward negative values, indicating
375 that the copper wire breaks on shipside, or toward high values (close to 35 °C or more), when the wire breaks
376 on probe-side where there is often a progressive increase in temperature values rather than a step transition to
377 full scale.

378

379



380 **Spike detection**

381 This test looks for single value spikes and it checks T measurements for large differences between adjacent
382 values. A spike is detected by computing the median value (Med_k) in a 5 points interval (3 m approximately)
383 with the profile value at the central point of the interval (T_k). The spike is detected and the consequent flag is
384 applied if T_k is not equal to Med_k and the difference (s_k) between T_k and the mean (Ave_k) in the chosen
385 interval is greater than a threshold value.

$$386 \quad Med_k = median(T_{k-2}:T_{k+2})$$
$$387 \quad Ave_k = mean(T_{k-2}:T_{k+2})$$
$$388 \quad s_k = T_k - Ave_k, c_k = T_k - Med_k \neq 0$$

389 The spike threshold values have been defined for the entire region in 5 vertical layers as the 99.9% quantile of
390 the s_k distribution and they are reported in Table 4. Figure 3a shows the probability distribution of s_k values
391 with c_k not equal to zero in 5 layers. s_k distribution is characterized by large values above 80 m that diminish
392 with depth, as the temperature variability does. The s_k scatter plot (Figure 3b) shows its values along the water
393 column, with the red dots highlighting the values over the selected thresholds.

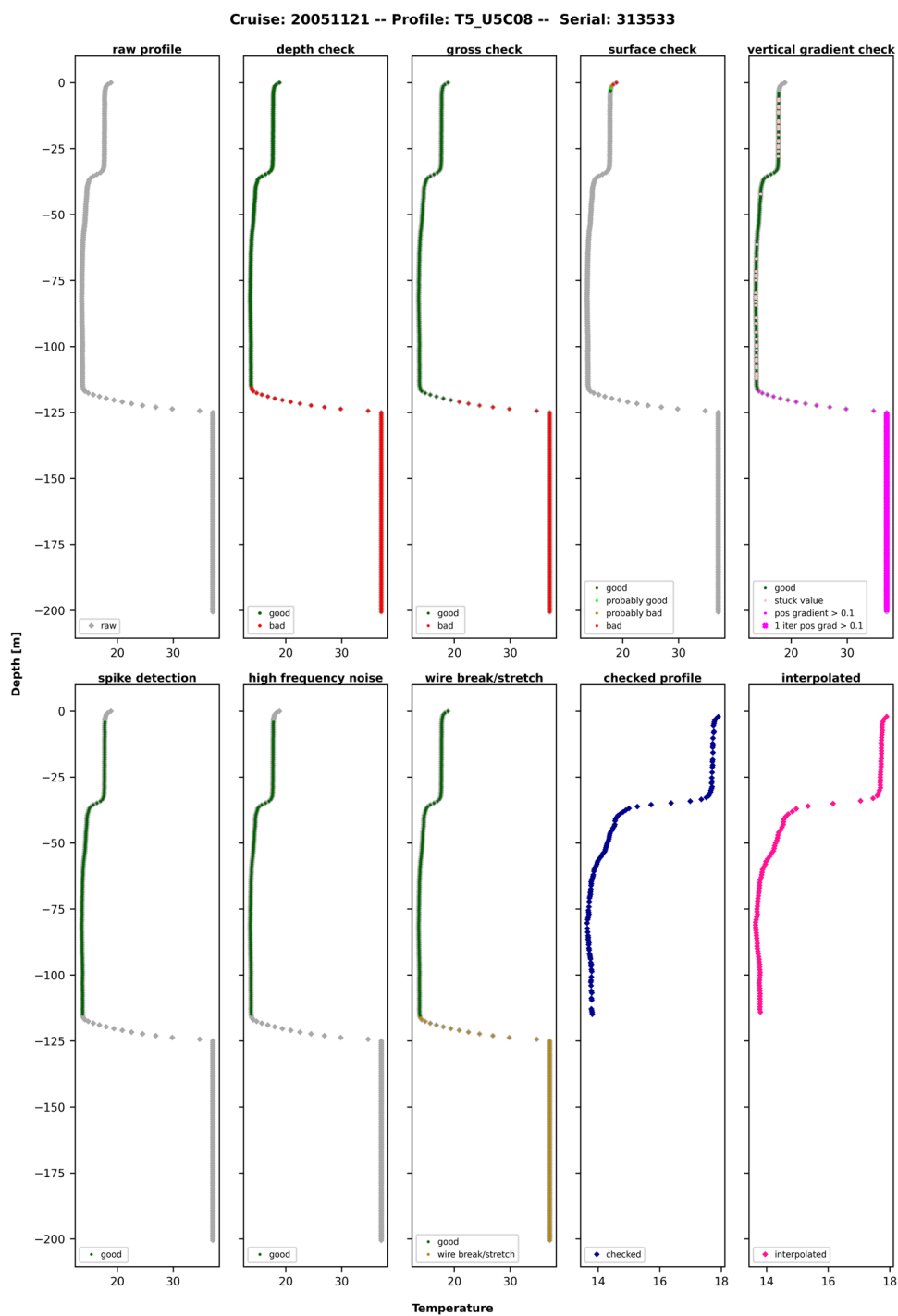
394 **Table 4 Spike detection threshold defined in 5 vertical layers.**

Layer	spike threshold (°C)
0-80 m	0.236
80-200 m	0.085
200-450 m	0.054
450-900 m	0.050
900-2300 m	0.022

395

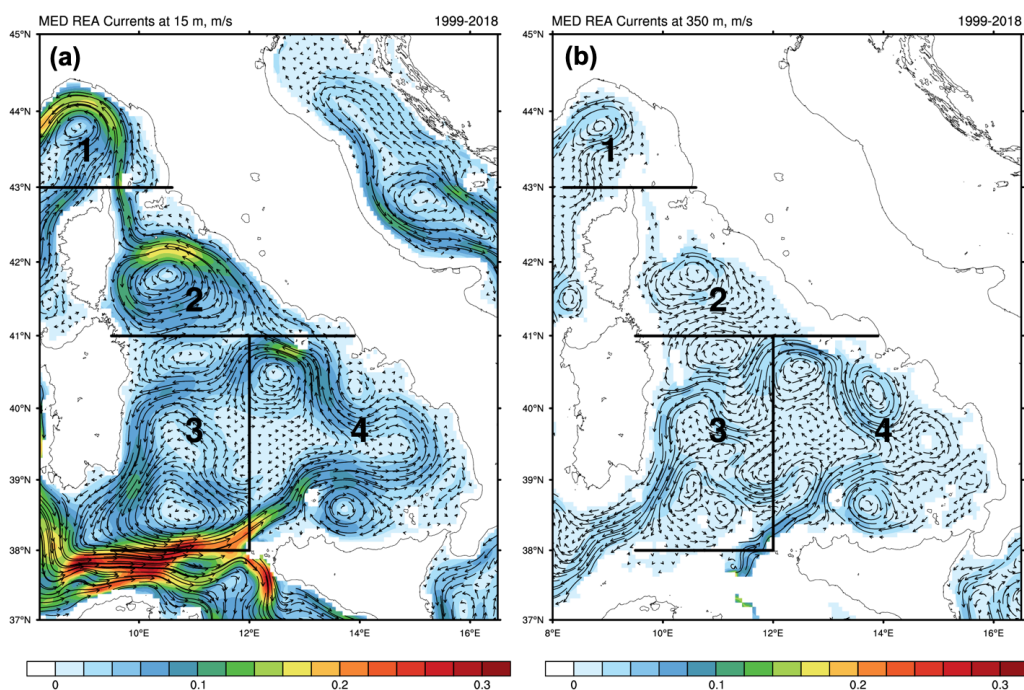
396 **High Frequency Noise**

397 It helps to identify critical T drops in the profile (such as large T differences over a large depth) by checking
398 continual spiking over a wide range of depths (Cowley and Krummel, 2022). In case of continual spikes, values
399 before and after a chosen interval (4 m approximately, i.e. 7 points) are tested considering the same acceptable
400 range of T inversion and gradient as in the *inversion and gradient checks* and flagged as bad if they are out of
401 the ranges.



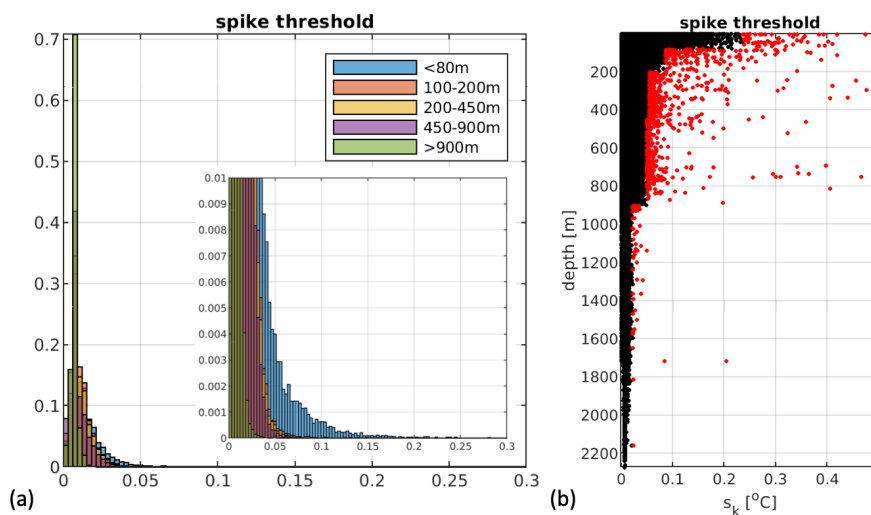
402

403 **Figure 2** Example of the quality flags generated by the automatic QC tests (Table 2) applied to a temperature
404 profile. The raw profile is at the top left and the final interpolated profile is at the bottom right.



405

406 **Figure 3** Maps of the mean circulation computed from the Mediterranean Sea reanalysis dataset (Simoncelli et al.,
 407 2014) at (a) 15 m and (b) 350 m.



408

409 **Figure 4** (a) Distribution in terms of probability of the spike threshold (s_k) in 5 layers with a zoom probability
 410 below 0.1%. (b) Vertical distribution of the spike threshold with indication in red the values above the 99.99%
 411 quantile.



412 4.2 Mapping QC test outcome to standard Quality Flags

413 Each basic QC test assigns a corresponding exit value or label to each original depth and T record (Table 3)
414 within the vertical profile and their mapping to QFs is necessary to allow the user to filter the original data
415 according to the quality requirements for the intended use. The QFs adopted, whose labels and corresponding
416 definition are reported in Table 5, have been selected from the SDN Common Vocabulary (IOC, 2013; IOC,
417 2019; <https://www.seadatanet.org/Standards/Common-Vocabularies>). The QF (Table 5) associated with each
418 original T measurement or depth value summarizes the results of the performed automatic tests and it is stored
419 in the dedicated ancillary variable (TEMPET01_FLAGS_QC or DEPTH_FLAGS_QC).

420 **Table 5 The Quality Flags (QF) selected from the SeaDataNet Common Vocabulary (IOC, 2013; IOC/UNESCO,**
421 **2019) assigned to the reprocessed XBT data.**

id	label	definition
1	good value	Good quality data value that is not part of any identified malfunction and has been verified as consistent with real phenomena during the quality control process
2	probably good value	Data value that is probably consistent with real phenomena but this is unconfirmed or data value forming part of a malfunction that is considered too small to affect the overall quality of the data object of which it is a part
3	probably bad value	Data value recognised as unusual during quality control that forms part of a feature that is probably inconsistent with real phenomena
4	bad value	An obviously erroneous data value
8	interpolated value	This value has been derived by interpolation from other values in the data object.

422

423 The general rule adopted for both depth and T QF is the following:

- 424 ● GOOD (QF=1) where all the tests pass;
- 425 ● BAD (QF=4) where at least one of the checks fails.

426 For T, we decided to use a higher level of detail, introducing also “probably good” (QF=2) and “probably bad”
427 (QF=3) flags, when it’s needed, since surface and inversion/gradient tests can provide more information on
428 profile behavior. After applying general rule for GOOD and BAD flags, we consider the flags coming from
429 the two mentioned tests and we update the flags as follows:

- 430 ● PROBABLY GOOD (QF=2) if the surface test returns a “probably good” flag;
- 431 ● PROBABLY BAD (QF=3) if the surface and/or the inversion test returns a “probably bad” flag.

432 Only measurements that have associated T and depth QFs equal to 1 or 2 have been used for the interpolation
433 at each meter depth. A relative QF associated to the interpolated profile has also been generated in order to
434 label (“interpolated value”, QF=8) when there is a gap of more than 5 consecutive points in the original profile,
435 which coincides with the number of points used to detect spikes (~3 m).



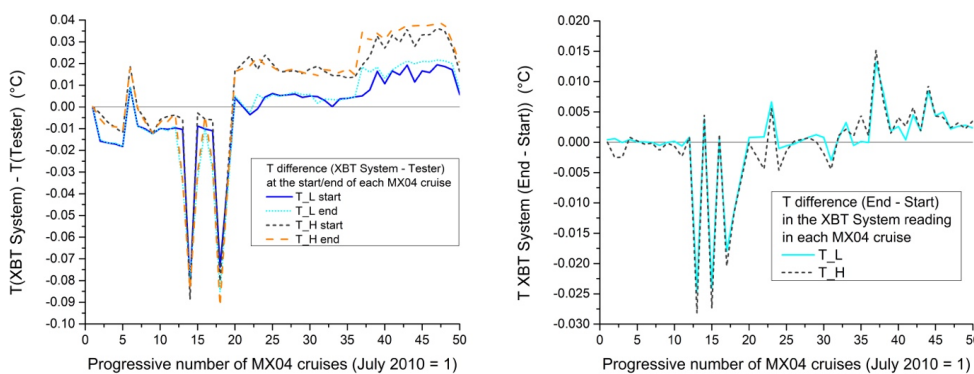
436 4.3 Calibration of the XBT system and correction

437 As previously highlighted, checking with a tester provides an assessment of the efficiency of an XBT system.
438 For example, Reseghetti et al. (2018) showed a notable improvement in the accuracy of XBT values compared
439 to measurements from a reference instrument (a CTD) in dedicated field tests when tester control correction
440 was applied.

441 The testers used here (built with high-performance resistors) have two reference temperatures (see Appendix
442 A for details). Once a tester is connected to an XBT system in a simulated drop, the tester's measurement
443 reading indicates how the XBT system's reading differs from nominal values at both temperatures. These
444 differences, which can be constant or variable over the time interval of data acquisition, can then be used to
445 correct the values of the XBT profiles.

446 The performance of the XBT system used was verified only for some subsets of the REP dataset. Since July
447 2010, a two-point tester has been used during cruises on the MX04 line with an initial check immediately
448 before the first drop and a final one after the last profile. Additional checks were performed whenever
449 computers or DAQ had failures. The differences measured at the reference temperatures at the start/end of
450 each MX04 cruise are shown in Figure 5a, while their drift during a cruise is in Figure 5b. It is well evident
451 that the values vary marginally and slightly over the time, but only in September 2013 (cruise 14) and June
452 2014 (cruise 18) large anomalies occurred for unknown reasons.

453



454 (a)

(b)

455 **Figure 5 (a) Temperature difference (XBT System-Tester) obtained from the checks at the reference temperatures**
456 **before starting and at the end of each MX04 cruise. (b) Difference between initial and final measurement with the**
457 **tester during the same cruise at the reference temperatures.**

458 4.3.1 Correction Algorithm

459 The measurements with a tester are used to correct the T values of each XBT profile of a campaign under the
460 assumption that the difference between the initial and final tester readings at reference temperatures varies
461 linearly over time from the beginning to the end of the campaign. The reference values are obtained by
462 calculating the average resistance value over the last 30 consecutive recorded values at each temperature in



463 the simulated drop (i.e. 3 seconds of acquisition, with a sampling frequency of 10 Hz) and then converted into
 464 T values (for details, see Appendix A). The differences between the nominal temperatures and the read values
 465 are linearly interpolated as a function of the time elapsed since the first launch to calculate their hypothetical
 466 value in correspondence with the k-th XBT probe during the campaign. In case of a single-point tester, a
 467 constant correction k-th is added to each value of the XBT profile k-th; while in case of two-point tester, the
 468 i-th correction is obtained by a further linear interpolation, based on the differences at upper and lower
 469 temperatures of this tester.

470 Notation:

- 471 • N is the number of XBT probes deployed during the campaign;
- 472 • T_+ and T_- nominal upper and lower temperature on the tester;
- 473 • $\Delta T_{+,i}$, $\Delta T_{+,f}$ initial and final temperature difference at the value T_+ ;
- 474 • $\Delta T_{-,i}$, $\Delta T_{-,f}$ initial and final temperature difference at the value T_- ;
- 475 • t_i , t_f initial and final time of the XBT drops (usually, t_i is set to 0);
- 476 • t_k time elapsed from the initial check with the tester, which is assumed to be coincident with the first
 477 XBT drop ($1 \leq k \leq N$);
- 478 • $T_{+,k}$ and $T_{-,k}$ theoretical upper and lower temperature that the tester should read at the k-th drop.

479 These last values can be calculated as

$$480 \quad T_{+,k} = T_{+,i} + \Delta T_{+,k} \quad \text{and} \quad T_{-,k} = T_{-,i} + \Delta T_{-,k}$$

481 where the estimated difference at upper and lower reference T corresponding at the k drop are:

$$482 \quad \Delta T_{+,k} = - \left[\Delta T_{+,i} + \left(\frac{\Delta T_{+,f} - \Delta T_{+,i}}{t_f - t_i} \right) (t_k - t_i) \right] \quad \text{and} \quad \Delta T_{-,k} = - \left[\Delta T_{-,i} + \left(\frac{\Delta T_{-,f} - \Delta T_{-,i}}{t_f - t_i} \right) (t_k - t_i) \right]$$

483 The so calculated contributions are combined in the correction term for the specific k-th XBT:

$$484 \quad \Delta T_{corr,k} = \left(\frac{\Delta T_{+,k} - \Delta T_{-,k}}{T_+ - T_-} \right) (T_{read,k} - T_-) + \Delta T_{-,k}$$

485 and then added the original value $T_{read,k}$ recorded by the DAQ:

$$486 \quad T_{corr,k} = T_{read,k} + \Delta T_{corr,k}$$

487 $T_{corr,k}$ is thus the value that best represents the actual seawater temperature measured by the k-th XBT probe
 488 assuming that the calculated correction (based on the initial and final measurements provided by the tester) is
 489 the best way to describe how the XBT system operates when the k-th probe was crossing the water column
 490 and measuring. Obviously, $\Delta T_{corr,k}$ cannot say anything about the quality of the measurement due to the
 491 characteristics of the k-th probe ("hot" or "cold" probe, or possible troubles during the acquisition).

492 When the calibration is available, the correction calculated in this way has been applied to the raw data prior
 493 to the QC analysis but it is also provided as a separate variable so that the user might decide to remove it. This
 494 correction must absolutely not be applied to the profiles from XCTD-1 probes because their acquisition circuit
 495 works in a completely different way and the shipboard DAQ simply acts as a data receiver and does not play
 496 an active role in the measurement.



497 **4.4 Vertical interpolation**

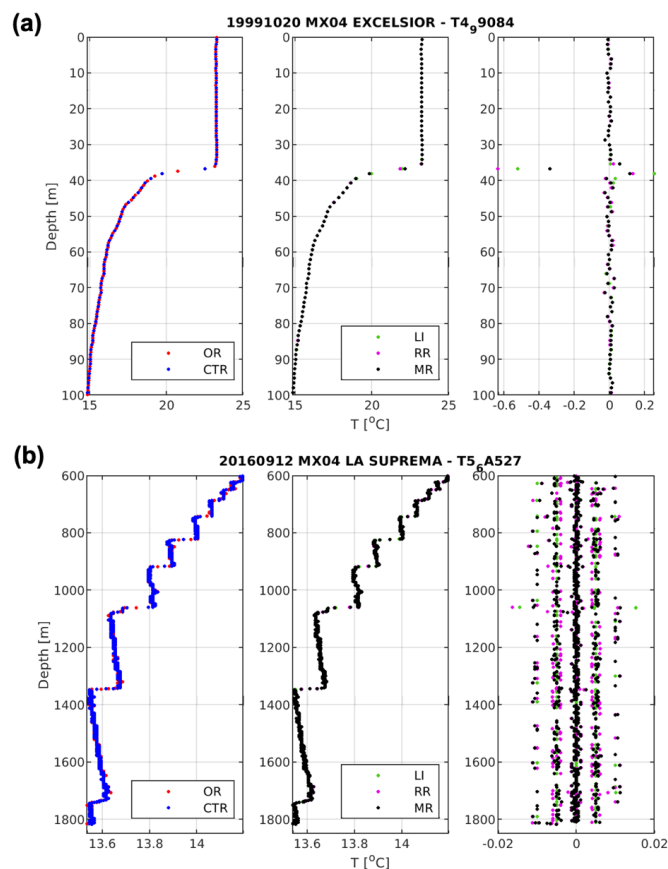
498 Three interpolation methods were tested: linear (LI), RR (Reiniger and Ross, 1968) and MR-PCHIP (Barker
499 and McDougall, 2020). The goal is to select the most conservative method, i.e. the one that provides the closest
500 interpolated T values to the original reading. The original measurements of each XBT profile were subsampled,
501 discarding half of the measurements then used as control values against the newly interpolated ones to calculate
502 differences and Root Mean Square Differences (RMSD) and therefore evaluate the best interpolation method
503 for our dataset.

504 Original values have been interpolated with the three methods on the control depth levels and the resulting T
505 estimates have been compared with the measured ones. Figure 6 shows an example of an observed profile with
506 highlighted control levels (magenta), the interpolated profile with the three considered methods and the relative
507 differences (interpolated-original). Figure 6a presents an example of the large T differences that occur between
508 interpolated and measured values (0.4 °C or -0.2 °C) along the thermocline at about 35 m. Figure 6b shows a
509 step-like profile below 600 m depth where the differences are very small, less than 0.02 °C, but they can
510 slightly increase and differ among the three methods where T vertical gradients occur.

511 Mean bias and RMSD have been computed in vertical bins (766) of 3 m thickness and the obtained metrics
512 profiles are displayed in Figure 7, associated with their relative vertical data distributions. These metrics have
513 been computed for the whole dataset and for two separate time periods: from June to November (when the
514 thermocline is well developed) and from December to May (when the water column is more homogeneous).
515 The mean bias in Figure 7 presents values in the range (-0.001,+0.001) °C, the interval halves from December
516 to May whereas it practically doubles (-0.002,+0.001) °C from June to November. The maximum RMSD when
517 considering all profiles is about 0.04 °C, it halves from December to May while it is close to 0.06 °C from June
518 to November. Except for the “mixed” plot, the maximum RMSD values are associated with LI and RR methods
519 but we note that $\text{RMSD} < 0.01$ °C for the three methods below 100 m depth.

520 The total RMSD on the entire water column has been summarized in Table 6 for the three time periods and
521 the surface layer above 100 m. In fact, the total bias estimated is zero for the three methods and the three time
522 periods, while the total RMSD is 0.011 °C for LI, 0.011 °C for RR and 0.010 °C for MR-PCHIP, while in the
523 surface layer the values are 0.023 °C, 0.021 °C and 0.019 °C respectively. The maximum RMSD values usually
524 occur during the stratified period (Jun-Nov) with values equal to 0.013 °C for LI, 0.012 °C for RR and 0.011
525 °C for MR-PCHIP, that in the surface layer become 0.030 °C, 0.027 °C and 0.023 °C, respectively.

526 The computed metrics in vertical bins present very small values, much lower than the nominal accuracy
527 associated with the measurements of an XBT system (0.2 °C). However, the absolute differences in the surface
528 layer when the thermocline settles can be larger than 0.2 °C as in Figure 6. The MR-PCHIP interpolation
529 always presents the smallest error for the analyzed dataset (Table 6) with respect to the reference values, thus
530 it has been applied to the REP dataset.

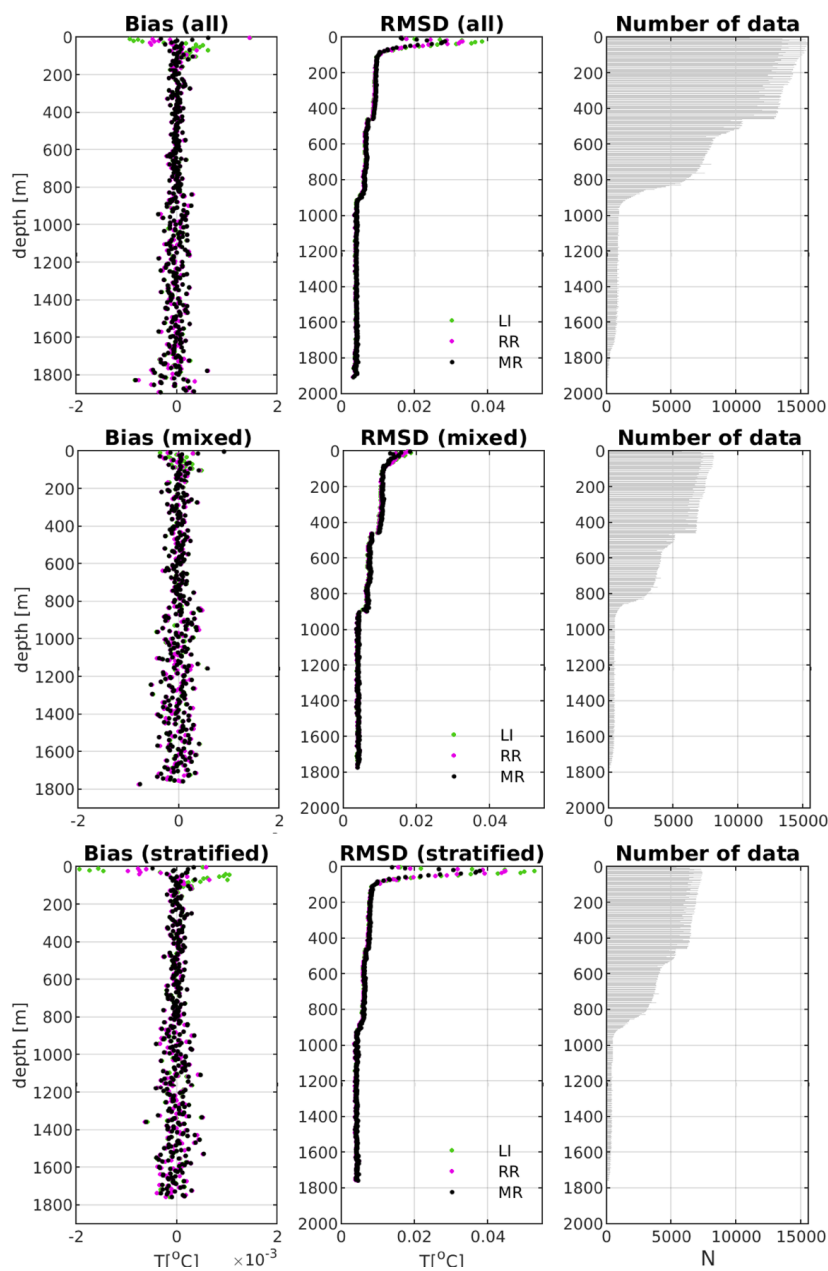


531

532 **Figure 6** Temperature profiles in the surface layer 1-100 m (a) and in the deep layer 600-1800 m (b): (left) magenta
 533 dots represent the control records; (middle) interpolated temperature values with linear LI (linear) , RR (Reiniger
 534 and Ross, 1968) and MR-PCHIP (Barker and McDougall, 2020); (right) differences between the interpolated and
 535 measured T values.

536 **Table 6** Summary of the computed metrics from the three interpolation methods: linear (LI), RR and MR-PCHIP
 537 Temperature RMSD [°C] have been computed in the entire water column and in the surface layer (0-100 m) from
 538 the whole dataset (All) and in two time periods December-May (mixed) and June-November (stratified).

RMSD	LI	RR	MR-PCHIP
All	0.011	0.011	0.010
0-100 m	0.023	0.021	0.019
Dec-May	0.010	0.010	0.010
0-100 m	0.014	0.014	0.013
Jun-Nov	0.013	0.012	0.011
0-100 m	0.030	0.027	0.023



539

540 **Figure 7** Profile of mean bias (left) and RMSD (middle) computed from profiles interpolated on selected depths
541 and compared to the corresponding measured values considering the three methods: linear (LI), Mr-PCHIP (MR)
542 and Reniger and Ross (RR). Three different time spans are shown: (top) the whole dataset; (middle) from
543 December to May; (bottom) from June to November. (right) Vertical data distribution in 3 m bins.



544 5. Results

545 The application of a series of QC algorithms to detect erroneous values is not capable of catching all of them.
546 According to Good et al. (2023) any automatic QC test produces a percentage of True Positives (TP, correctly
547 detected erroneous data) and False Positives (FP, incorrectly detected erroneous data) and the general aim
548 would be to maximize the TP (correct flagging) rate and minimize the FP (incorrect flagging) rate.

549 The new automatic QC procedure has been deeply tuned by visual check to reach an optimal TP/FP rate. In
550 specific, efforts have been made to tune the vertical gradient and spike thresholds, tuned by quantiles analysis,
551 to maximize the detection of erroneous data and minimize to flag as BAD data the GOOD ones. This was
552 particularly tricky for the vertical gradient test which detected 121 profiles with out of bounds values, but 28
553 of them appeared FPs (FP/TP rate of 23%) from visual check. In fact, the strong seasonal stratification of the
554 Mediterranean Sea and the presence of several water masses in different water layers might cause the incorrect
555 flagging as BAD of GOOD data, as shown in Figure 8b,d. This makes the vertical gradient test non-optimal
556 for the Mediterranean Basin with a high FP rate, thus a very small percentage associated with the quantiles
557 have been selected to minimize this.

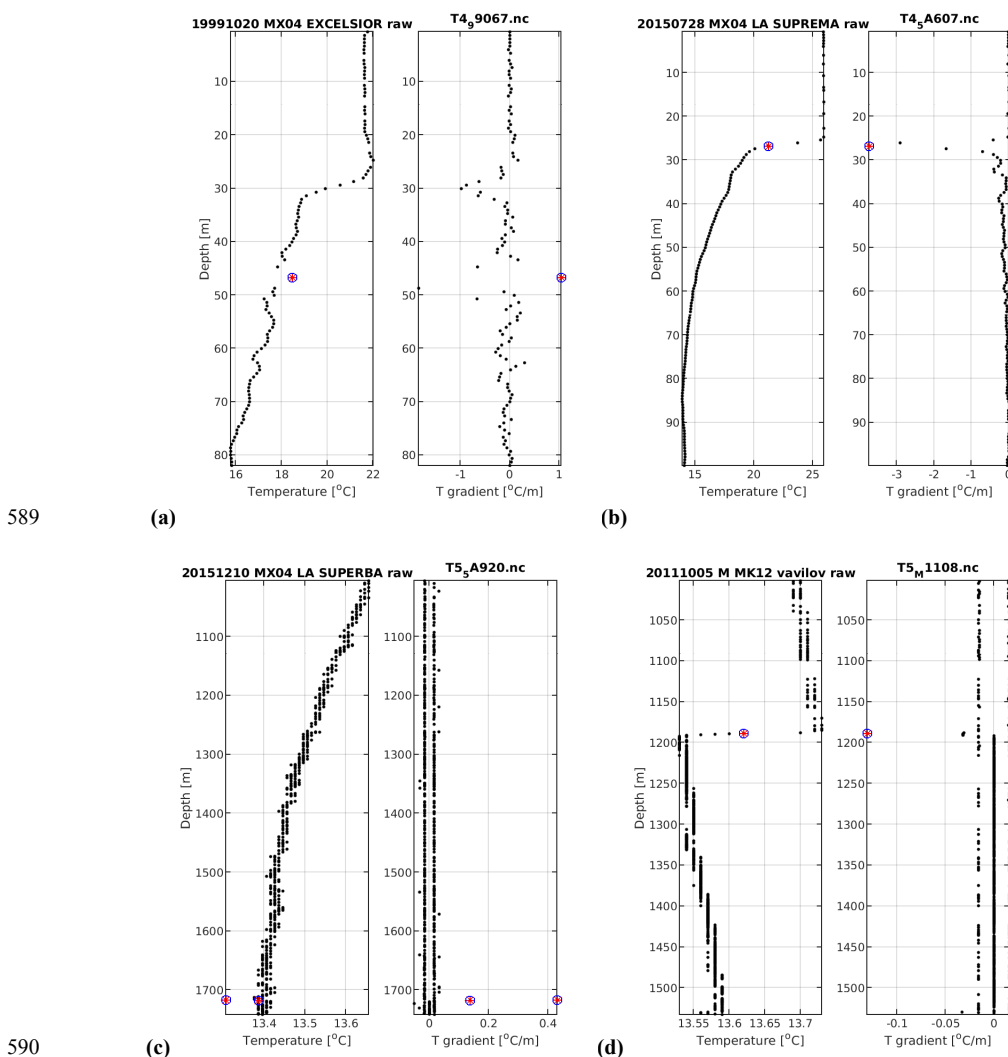
558 The spikes test instead is much more effective (331 profiles with detected spikes of which 11 are FPs),
559 providing a low FP/TP rate (3.3%). Figure 9 shows example profiles with true spikes (a) and wrong spikes (b),
560 mainly marked at the start of the thermocline

561 However, some profiles present anomalous features that automatic QC procedure could not detect. The
562 decision was to add a flag associated with the whole profile indicating the depth range where unrecoverable
563 problems happened or began. The indispensable premise is the knowledge of the main physical characteristics
564 of the water masses present in the analyzed region. In fact, the very small value of the Rossby radius (≤ 11.5
565 km irregardless of the season) and the occurrence of repeated and well-documented thermal inversions must
566 always be considered when the quality of the T profiles is analyzed. Step-like structures (“staircases”) are also
567 typical of the southern Tyrrhenian Sea, explained usually in terms of the double diffusion process (Meccia et
568 al. 2016; Durante et al., 2021).

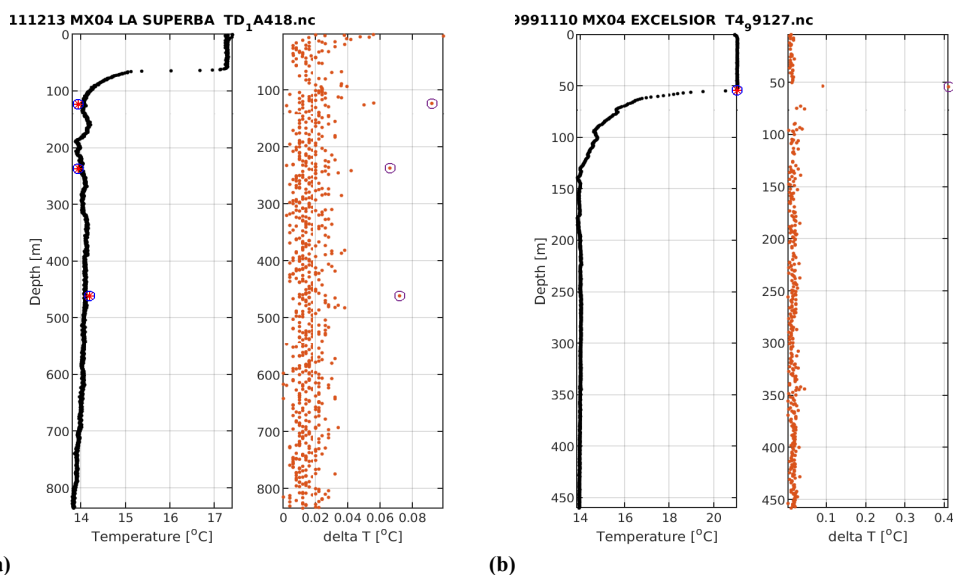
569 Sometimes, the meteorological conditions and a non-accurate knowledge of the bathymetry can make the
570 expert validation of XBT profiles difficult, but their extreme variability can also be ascribed to multiple
571 instrumental and operational factors. In every XBT drop, the correct unwinding of the wire from both spools,
572 adequate and complete protection of the insulating substance along its entire length are essential to guarantee
573 good quality of the recorded data. For example, most profiles from XBTs launched from ships traveling at low
574 speed (i.e. $v < 15$ knots) are generally less affected by significant electrical disturbances, even in the presence
575 of non-zero wind. Unfortunately, the ships used on the MX04 line (from which most of the REP profiles
576 belong) have a standard speed close to 22 knots and this makes the acquisition conditions vulnerable. The XBT
577 profiles from containerships also have a lower quality due to the usually very high launch position ($h > 25$ m),
578 which also makes the probe depth in the initial measurements provided by software questionable (Bringas and
579 Goni, 2015). An XBT, during acquisition, due to the electric current present in the copper wire, acts as an
580 antenna sensitive to all electromagnetic phenomena occurring in the atmosphere in a region close to the



581 launching position and on the ship. The occurrence of atmospheric events (thunderstorms with lightning), even
582 at a relative distance from the ship, can have a non-negligible impact on the "cleanliness" of the recorded
583 signal, same as the proximity to on-board instrumentation producing significant electromagnetic fields and
584 whose operation is random. The physical parameter measured by the XBT system is the electrical resistance,
585 which has two components: one is from the wire and the other from the NTC thermistor which falls through
586 the water column. Gusts of wind combined with turbulence produced by the ship hull can produce "whiplash"
587 on the copper wire and badly influence the shape of the profiles collected with particularly unfavorable wind
588 conditions.



591 **Figure 8** Examples of temperature gradient flags applied to different XBT profiles: (a) true positive vertical
592 gradient anomaly in the surface layer; (b) true positive vertical gradient anomaly in the surface layer; (c) true
593 positive vertical gradient anomaly in the bottom layer; (d) false positive vertical gradient anomaly in the bottom
594 layer.



595

(a)

(b)

596 **Figure 9** Examples of spikes detected in two different XBT profiles: (a) true spikes; (b) false spike at the start of a
597 steep thermocline. The orange dots in the right panels of (a) and (b) indicate the estimated value of the s_k parameter
598 having c_k not equal to zero.

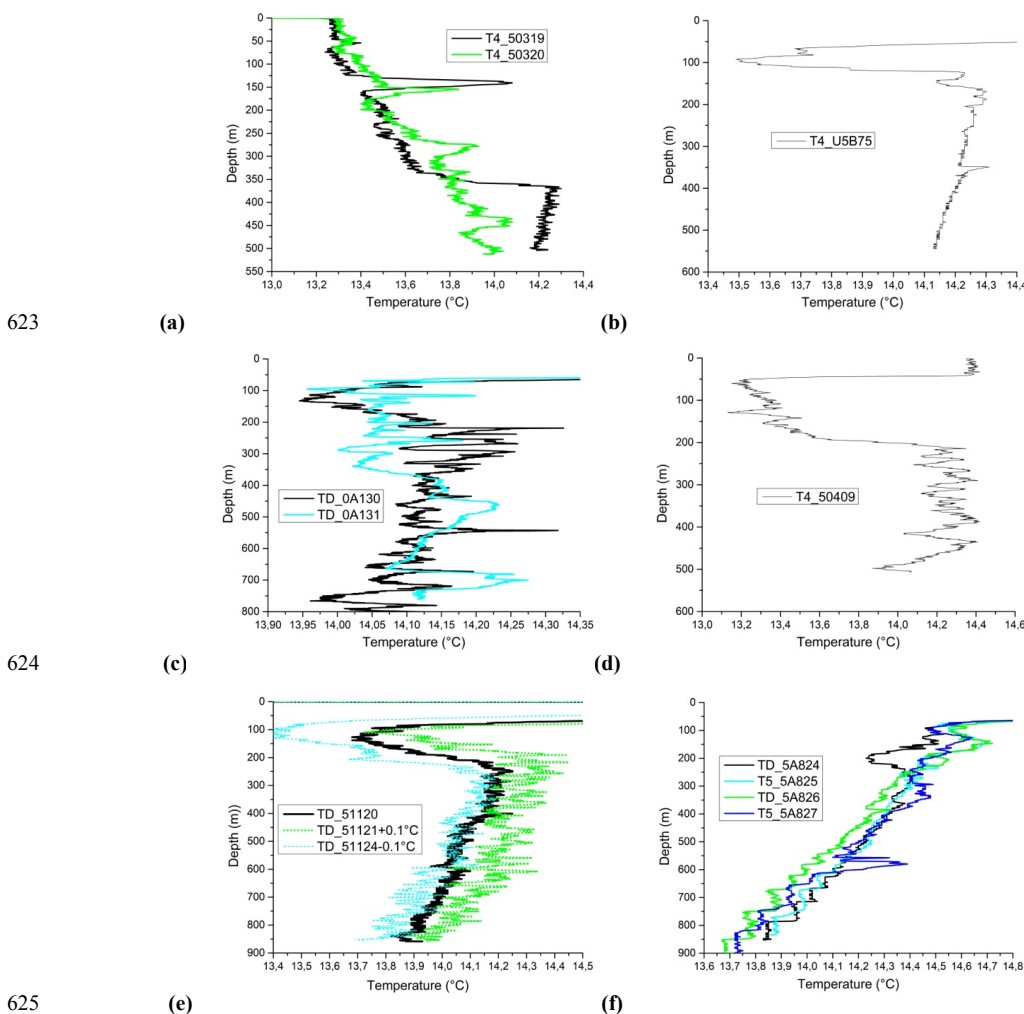
599 A difficult task has been how to identify these external influences that induce “oscillations” in the shape of T
600 profile, as in the examples of Figure 10 c-d-e, and how to annotate it in the metadata. Some other anomalous
601 "thermal structures", compared to what is expected in a certain period, region and depth layer are shown in
602 Figure 10 a-b and f (anomaly around 400 m depth in the blue profile and at 550 m in the green one). The
603 "visual check" carried out by the expert allows in some cases to highlight notable deviations in the shape and/or
604 values of a profile compared to adjacent ones. The probability of having the same type of "anomalous"
605 structure recorded by two adjacent XBT probes in time and space is considered negligible, favoring the
606 occurrence of something "physical" instead of non-optimal functioning of a specific probe. Sometimes the
607 initial “BAD” attribution to anomalous structures was subsequently reviewed by the comparison with adjacent
608 profiles that present something similar.

609 5.1 Validation with SeaDataNet version

610 A significant part of the XBT profiles included in this dataset have been systematically disseminated through
611 the SDN infrastructure and can be accessed from the data access portal through the saved query Url
612 https://cdi.seadatanet.org/search/welcome.php?query=1866&query_code={4E510DE6-CB22-47D5-B221-7275100CAB7F}). Alternatively, they can be found in the Mediterranean aggregated dataset product
613 (Simoncelli et al., 2020a) in which they are integrated with other data types (CTDs, bottles, MBTs, profiling
614 floats). This data product has been further validated in the framework of the SeaDataCloud project
615 (https://www.seadatanet.org/About-us/SeaDataCloud), as described in Simoncelli et al. (2020b).



617 The SDN XBT dataset, extracted from Simoncelli et al. (2020a) is considered here as a benchmark to highlight
618 the main effects of the proposed data reprocessing. Bias and RMSD profiles have been computed from 3104
619 matching profiles with a vertical data distribution shown in Figure 11. Since SDN profiles do not have the
620 calibration correction, we have computed the separate metrics with and without the correction applied. The
621 black dots represent all matching profiles, green dots represent the profiles without correction and the red dots
622 have the correction applied.

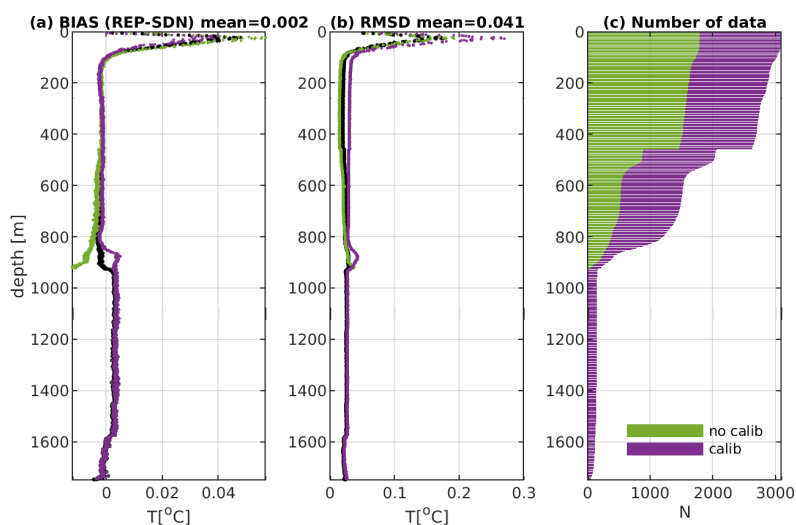


626 **Figure 10** Examples of profiles with critical features. Remark: the axes ranges are different and selected to
627 highlight some peculiar structure. The name of the selected profile(s) is shown in the legend.

628 The maximum discrepancy among the two data versions resides always within the surface layer until 150 m
629 depth. The maximum bias and RMSD reach approximately 0.05 °C and 0.2 °C respectively, which might imply
630 potential significant changes in downstream applications. The bias is larger (~0.06 °C) when estimated from
631 profiles without correction and slightly smaller (~0.04 °C) from non-corrected profiles, while the largest



632 RMSD derives from profiles with the correction applied, indicating that the correction slightly increases on
633 average the REP temperature values and consequently the positive bias.
634 The REP profiles are warmer than SDN ones in the surface layer and below 900 m, while between 150 m and
635 800 m both metrics are small and quite constant. The overall mean bias and RMSD are equal to 0.002 °C and
636 0.041 °C, respectively. The sharp reduction in the number of observations available below about 900 m depth
637 could affect the shape of both BIAS and RMSD profiles.
638 Such differences are mainly due to the new interpolation technique, the lack of filtering, the application of the
639 calibration correction in the REP dataset, and in very few cases, the use in SDN of wrong FRE coefficients or
640 the incorrect probe type assignment which can produce a change of the depth values.

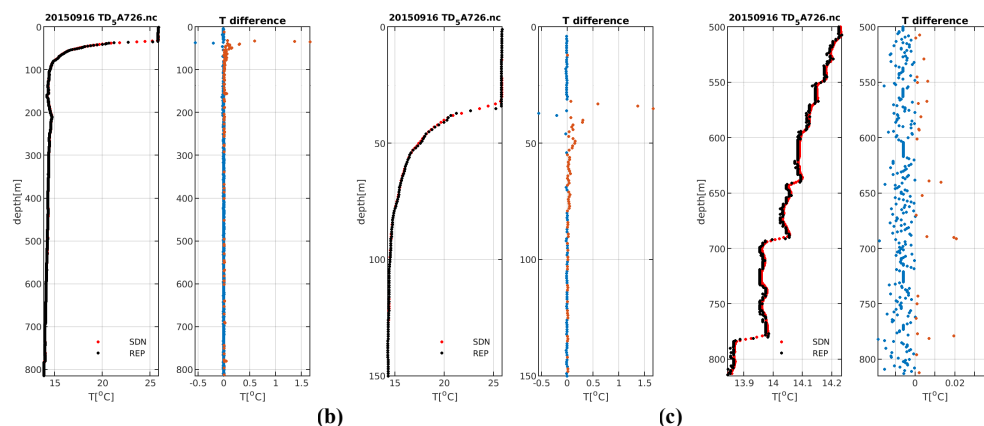


641

642 **Figure 11 Comparison between the reprocessed (REP) and the corresponding SeaDataNet (SDN) profiles at each**
643 **meter depth: (a) Bias mean profile; (b) RMSD profile and (c) cumulative vertical data distribution which shows**
644 **the relative contribution of profiles with calibration and profiles without calibration to the total.**

645 Figure 12 shows an example of matching REP and SDN profile and the relative differences at each meter of
646 depth (a) with a zoom in the surface (b) and bottom layers (c), where the largest differences occur. During the
647 stratified period, the largest differences reside in the thermocline and can exceed 1.5 °C, while in the bottom
648 layer the frequent step-like shape of the profile, due to double diffusion processes (Meccia et al. 2016; Durante
649 at al., 2021), explains the positive average bias in Figure 11a.

650 In the SDN dataset, the interpolation of raw profiles at each meter depth has been combined with the
651 application of a Gaussian filter to reduce possible noise (Manzella et al., 2003 and 2007). Consequently, a
652 general smoothing of T profiles is observed, which is appreciable to remove/reduce unrealistic high frequency
653 oscillations, if needed, but it also affects the values of the whole profile. The main effect is that the shape of
654 thermal structures is smoothed out, more or less evidently depending on the recorded T gradient.



655 (a) (b) (c)
656 **Figure 12** Example of a reprocessed (REP) profile and the corresponding SeaDataNet (SDN) one: (a) whole profiles
657 on the left and relative difference profile on the right; (b) zoom in the surface layer 0-150 m (c) zoom in the bottom
658 layer 500-800 m.

659 6. Summary and Conclusions

660 This work presents the reprocessing of XBT profiles in the Ligurian and Tyrrhenian Seas over the time period
661 1999-2019. The added value of this analysis is the availability of the original raw data and all the metadata
662 from the operational manual notes. This allowed us to create the most complete dataset possible with metadata
663 accompanying each individual T profile. The surface measurements have been added with quality indication
664 and a correction from calibration has been applied, when available, to T values (generally in the range 0.01-
665 0.02 °C), representing the best estimate of the thermal offset due to the operating XBT system characteristics.
666 A new automatic QC procedure and a new vertical interpolation (Barker and McDougall, 2020) have been
667 implemented without the application of any filter that: on one side, removes unrealistic high frequency
668 oscillations, and on the other, it smooths out the thermal structure of the T profiles with main impact on the
669 surface layer during stratified conditions. The adoption of a Gaussian filter from Manzella et al. (2003, 2007)
670 was justified by the purpose of assimilating XBT profiles in the Mediterranean Forecasting System that in the
671 early 2000s was characterized by a much lower resolution compared to the present numerical model
672 capabilities. The REP dataset gives researchers the most complete information for its re-use for different
673 applications (assimilation in ocean and climate models, process and climate studies). It can also be used to test
674 new QC algorithms or the order on which to apply them to further improve the data quality.

675 The adoption of FAIR data management principles through the use of SeaDataNet standards and the
676 dissemination strategy based on the ERDDAP server implementation are additional values of this effort,
677 allowing its machine to machine access.

678 XBTs are a 60-year-old technology. Though the quality of their measurements might not fit the purpose of all
679 applications and they leave debris in the ocean, “XBTs provide the simplest and most cost-efficient solution
680 for frequently obtaining temperature profiles along fixed transects of the upper ocean” (Parks et al., 2022)
681 using ships of opportunity. Moreover, the XBT measurements along the MX04 track were for some periods



682 among the few measurements recorded in the Tyrrhenian and Ligurian Seas. Despite the limitations of the
683 XBT characteristics, they constituted the simplest way to verify the physical state of the upper layer of those
684 basins. It is therefore very important to provide those profiles with the best quality and usability indications.
685 For this reason, the MX04 line has been re-established in the framework of the MACMAP project after a two-
686 year break on a seasonal base for climate monitoring.
687 In recent years, the use of XBTs has also been criticized because all probe components fall to the seabed.
688 Given the current MACMAP sampling strategy with 37 launches in a fixed and determined position, the
689 quantity of material abandoned at sea for each campaign can be easily estimated (about 22 kg of ZAMAK, just
690 over 2 kg of plastic and about 11 kg of copper wire). If the XBT probes were made with other materials (e.g.,
691 iron "nose" and biodegradable plastic components), it would certainly be better. However, in a cost-benefit
692 balance, the environmental impact due to the collection of profiles included in this dataset is exceeded by the
693 scientific results. The use of XBTs allows the planning of monitoring surveys with only 24-36 hours advance
694 notice, along a specific path including coastal areas, using merchant vessels. The MX04 transect has provided
695 a series of tomographic-like "thermal images" along essentially the same path since September 1999,
696 monitoring the area over the years and the occurrence of transient events and their evolution to be analyzed.
697 Finally, the deployment of the XBT probes described here did not contribute to additional emissions of CO₂
698 and other atmospheric pollutants, because only commercial vessels were used and in the case of research
699 vessels, the launch of the XBT probes was ancillary to the primary activities for which the campaign was
700 planned.

701 **7. Data Availability and FAIRness**

702 The management of the REP dataset has been conceived since the beginning to be compliant with the FAIR
703 (Findable, Interoperable, Accessible, Reusable) data management principles (Wilkinson et al., 2016) and the
704 open science paradigm. The REP dataset (Reseghetti et al., 2023;
705 https://doi.org/10.13127/rep_xbt_1999_2019) is available and accessible through INGV (Bologna) ERDDAP
706 server (<http://oceano.bo.ingv.it/erddap/index.html>), which allows machine to machine data access and gives
707 to the users the possibility to select among several download formats. The raw data with complete metadata
708 description and the interpolated data after data QC are released together with all the processing information in
709 order to facilitate data reuse. The format and the standards adopted for the dissemination of the REP dataset
710 are described in detail in Appendix C. The ODV collection of the REP interpolated dataset, used for the visual
711 check, is also available on request.

712

713 **Author contribution**

714 SS conceptualized the work, FR curated the original data (collecting a significant portion of it), CF developed
715 the QC software, under the methodology supervision of SS, FR and LC. GR prepared the correction from the
716 calibration of DAQs. CF manages and curates the reprocessed dataset. SS, FR and CF prepared the manuscript
717 with contributions from GR and LC.



718

719 **Competing interests**

720 S. Simoncelli is a member of the editorial board of the journal. Co-authors declare that they have no conflict
721 of interest.

722 **Acknowledgements**

723 We thank all people/institutions/companies involved in the data taking:

- 724 ● The Italian shipping company GNV (Grandi Navi Veloci), a very special partner that has allowed the
725 monitoring activity since September 1999: in particular Marco Fasciolo, Dr. Mattia Canevari, the
726 captains, the officers and all the crews for their precious collaboration;
- 727 ● Persons involved in data collection on the MX04 line, namely M. Borghini, F. Dell'Amico, C.Galli,
728 E. Lazzoni (CNR-ISMAR), M. Morgigni and A. Baldi (ENEA);
- 729 ● CNR-ISMAR-Lerici for the very long collaboration that has allowed the acquisition of numerous XBT
730 profiles from research vessels, in particular the crew and technicians of the RV Urania;
- 731 ● The international shipping companies Hapag Lloyd, CMA CGM and Arkas, their managers and crews
732 for their valuable collaboration;
- 733 ● Responsible officers ashore and on board, crews and technicians of ships belonging to IIM, in
734 particular CF Maurizio Demarte and Dr. Luca Repetti.
- 735 ● Australian government agency CSIRO for its kind cooperation by sharing their instrumentation in the
736 2007-2011 data collection on container ships, notably Dr. Ann Thresher, Dr. Lisa Krummel and Dr.
737 Rebecca Cowley;
- 738 ● The Federal Research Laboratory NOAA-AOML of Miami (FL), in particular Dr. Gustavo Goni and
739 Dr. Francis Bringas, for the supply of the XBT probes used during some MX04 campaigns and for the
740 support in carrying out the operational activities;
- 741 ● Stefano Latorre (INFN, Milan), key person in the development and implementation of the testers and
742 their periodic calibration;
- 743 ● One of the authors (FR) for having supplied his own instrumentation and XBT probes for carrying out
744 oceanographic campaigns since 2008.

745 A very special thanks to Giuseppe M. Manzella, who created the SOOP program in the Mediterranean Sea and
746 coordinated it until 2013. He supported this paper, providing useful comments.

747 We acknowledge Marjahn Finlayson for reviewing the English, and Mario Locati (head of the INGV data
748 management office) for his continuous support. This work has been developed in the framework of the
749 MACMAP project, funded by Istituto Nazionale di Geofisica e Vulcanologia (Environment Department), and
750 coordinated by Antonio Guarnieri that we thank.

751



752 **Appendix A**

753 **Characteristics of test canisters**

754 While in the laboratory, it is easy to have environmental conditions constant and under control for
755 measurements, in the field, this is only an aspiration of the operators. Furthermore, repeated operation in
756 conditions of high temperature, humidity and salinity certainly does not facilitate the proper functioning of the
757 electronic instrumentation. The DAQ in an XBT system should read (within the uncertainties of the
758 measurements) the nominal value of a resistance showing no changes in its reading over time because it is an
759 essential component to get good quality XBT measurements. The use of a tester with high quality resistors is
760 the preferred method to verify this. Between 2007 and 2010, two testers were built using very high precision
761 resistors (model KOA-Speer RN73r1jtttd1002b10) combined in such a way as to achieve corresponding T
762 values similar to the extreme ones measured in the marine regions under investigation. The resistance values
763 of both testers were checked each year with a Wavetek Datron 1281 8.5 digits multi-meter in a laboratory of
764 the INFN (Italian National Institute of Nuclear Physics) in Milan (room temperature always in the range 20-
765 24 °C during measurements). The reading remained stable (within 0.1 Ohm) over the period 2008-2019 for
766 the former and 2010-2015 for the latter.

767 **Table A1 - The resistance values measured in the control tests with the corresponding temperature values**
768 **calculated by a Hoge_2 equation for the two testers used in the XBT data acquisition campaigns since 2010.**

Model	Resistance 1 (Ohm)	Temperature 1 (°C)	Resistance 2 (Ohm)	Temperature 2 (°C)
Test canister 1	4631.0 ± 0.1	26.758 ± 0.001	8960.1 ± 0.1	12.197 ± 0.001
Test canister 2	4397.2 ± 0.1	27.956 ± 0.001	8725.3 ± 0.1	12.759 ± 0.001

769

770 The resistance R values shown in Table A1 are then converted to T by applying the Hoge_2 R to T equation
771 (Sippican, 1991 and 2010; Hoge, 1988; Chen, 2009; Liu et al., 2018) with the following coefficients:

772 $A = 1.2901230e-3$

773 $B = 2.3322529e-4$

774 $C = 4.5791293e-7$

775 $D = 7.1625593e-8$

776 This equation and the associated coefficients remained unchanged since the 1990s for all the DAQs used.

777



778 **Appendix B**

779 **Table B1 - Some details of instrumentation and operating conditions during the collection of the XBT profiles**
 780 **included in the REP dataset for all the ships participating the measurements.**

Ship Name	Call Sign/ IMO No.	Number of Campaigns	Years of Activity	DAQ used	Height launch (m)	Range of ship speed (knots)
Excelsior	IBEX 9184419	20 1 7	1999-2000 2012 2017-2018	MK12 MK21 USB MK21 Ethernet	10±0.5	20-24
Excellent	IBBE 9143441	1 5	2004 2012-2014	MK21 ISA MK21 USB	10±0.5	19-24
Splendid	IBAS 9015747	1	2011	MK21 USB	10±0.5	20-22
La Superba	ICGK 9214276	14 1 23 1 3	2004-2006 2010 2010-2016 2011 2016-2017	MK21 ISA TURO QUOLL MK21 USB MK12 MK21 Ethernet	11±0.5	21-28
La Suprema	IBIL 9214288	2 6 6	2004 2011-2016 2016-2019	MK21 ISA MK21 USB MK21 Ethernet	11±0.5	21-28
Wellington Express	DFCX2 9224051	5	2007-2008	TURO DEVIL	25±1.0	14-20
Canberra Express	DFCW2 9224049	1	2008	TURO DEVIL	25±1.0	14-20
Stadt Weimar	DCHO 9320051	8	2009-2010	TURO DEVIL	27±1.0	14-20
CMA CGM Charcot	A8HE4 9232773	5	2009-2011	TURO DEVIL	25±1.0	14-20
Daniel A	TCLA 9238064	2	2014	MK21 USB	8±0.5	14-17
Ammiraglio Magnaghi	IGMA 8642751	3 1 2	2008-2013 2011 2019	MK12 MK21 USB TURO QUOLL	(3 – 6) ±0.5	1-10
Aretusa	IABA	1 2	2006 2017-2018	MK12 MK21 USB	(4 – 5) ±0.5	1-10
Galatea	IABC	1	2013	MK12	(4 – 5) ±0.5	1-10
Urania	IQSU 9013220	12 13	2000-2012 2005-2014	MK12 MK21 USB	(3 – 12) ±0.5	0-11
Minerva 1	IZVM 9262077	1 1	2015 2016	MK21 USB MK21 Ethernet	(3 – 8) ±0.5	0-11
Ibis	--	1	2019	MK21 Ethernet	3 ±0.5	0-10

781

782



783 **Appendix C**

784 **Format and standards**

785 The data format adopted to archive the REP dataset is the netCDF (Network Common Data Form). It is self-
786 describing since it includes the metadata that describe both data and data structures. The NetCDF
787 implementation is based on the community-supported Climate and Forecasts (CF) specification (CF1.6 profile
788 for point data) and it adopts the SeaDataNet (SDN) vocabularies
789 (<https://www.seadatanet.org/Standards/Common-Vocabularies>). The reference SDN parameter codes (P01
790 terms, https://vocab.seadatanet.org/v_bodc_vocab_v2/search.asp?lib=P01) and the associated standard units
791 (P06 terms https://vocab.seadatanet.org/v_bodc_vocab_v2/search.asp?lib=P06) are used in order to ensure the
792 proper interpretation of values by both humans and machines and to allow data interoperability in terms of
793 manipulation, distribution and long-term reuse.

794 Each XBT NetCDF file contains:

- 795 • **dimensions** that provide information on the size of the variables (a.k.a. “parameters”);
- 796 • **coordinate variables** that orient the data in time and space;
- 797 • **geophysical variables** that contain the actual measurements;
- 798 • **ancillary variables** that contain the quality information (Quality Flags, QFs) values;
- 799 • **additional variables** that include some of the variables being part of SDN extensions to CF;
- 800 • **global metadata fields** that refer to the whole file, not just to one variable (a.k.a. “global attributes”).

801 **C.1 Dimensions**

802 The pattern followed by SDN for “profiles” data type is to have an ‘INSTANCE’ unlimited dimension plus a
803 maximum number of z coordinate levels (*MAXZ*). We included also string size dimension STRING for text
804 arrays and added test size dimensions referring respectively to test QFs on temperature (*TST_T*) and depth
805 (*TST_D*) values and the maximum number of z coordinate levels for the data re-sampled at a 1 m interval, after
806 the Quality Check (QC) is applied (*MAX_INT*).

807 **C.2 Coordinate variables**

808 NetCDF coordinates are a special subset of variables which orient the data in time and space. They are:

- 809 • *LONGITUDE* for x;
- 810 • *LATITUDE* for y;
- 811 • *TIME* for t;
- 812 • *DEPTH* for z.

813 **C.3 Geophysical variables**

814 Each file contains:



- 815 • full resolution raw Temperature (T) data corrected via calibration based on tester check (when
816 available) and,
817 • interpolated data at each meter depth

818 Calibration values are provided in a separate variable as well, so that experts can trace back the raw
819 (uncalibrated) profile if needed.

820 For each coordinate and geophysical variable four mandatory parameter attributes are included, as defined in
821 Lowry et al. (2019):

- 822 1. *sdn_parameter_urn*: this is the URN for the parameter description taken from the P01 vocabulary;
- 823 2. *sdn_parameter_name*: this is the plain language label (Entryterm) for the parameter taken from the
824 P01 vocabulary at the time of the data creation;
- 825 3. *sdn_uom_urn*: this is the URN for the parameter units of measurement taken from the P06 vocabulary;
- 826 4. *sdn_uom_name*: this is the plain language label (Entryterm) for the parameter taken from the P06
827 vocabulary at the time of data file creation.

828 Moreover, since some of the coordinate variable names could be ambiguous, particularly for the z-coordinate,
829 we adopt the *standard_name* (P07 vocabulary,
830 https://vocab.seadatanet.org/v_bodc_vocab_v2/search.asp?lib=P07), not mandatory in CF but widely used,
831 which significantly enhances interoperability.

832 C.4 Ancillary variables

833 In order to report data quality information on a point by point basis, every measurement is tagged with a single-
834 byte encoded label referred to as a ‘flag’. The flag variables are mandatory for all coordinate and geophysical
835 variables to which they relate through ‘ancillary_variables’ in the parent variable set to the name of ancillary
836 variable attribute (Lowry et al., 2019). The flags are encoded using the SDN L20 vocabulary
837 (https://vocab.seadatanet.org/v_bodc_vocab_v2/search.asp?lib=L20) and each ancillary variable carries
838 attributes ‘flag_values’ and ‘flag_meanings’, which provide a list of possible values and their meanings.

839

840 For coordinate variables, the ancillary variables are the following:

- 841 • *TIME_SEADATANET_QC*: it is the ancillary variable referring to *TIME* parent variable;
- 842 • *POSITION_SEADATANET_QC*: Longitude and latitude flag variables are combined into a single
843 flag for ‘position’, following OceanSITES (2020) practice. .

844

845 For depth coordinate, there are three different ancillary variables:

- 846 • *DEPTH_TEST_QC*: it contains flags coming from the application of depth check test;
- 847 • *DEPTH_FLAGS_QC*: it contains flags associated with each original depth value and summarizes the
848 results of the performed depth test check mapped on SDN L20 vocabulary;
- 849 • *DEPTH_INT_SEADATANET_QC*: it contains flags associated with the interpolated profile.

850



851 For temperature geophysical variable, the ancillary variables, similarly to depth coordinate, are the following:

- 852 • *TEMPET01_TEST_QC*: it contains flags coming from the application of independent temperature
853 check tests;
- 854 • *TEMPET01_FLAGS_QC*: it contains flags associated with each original temperature value and
855 summarizes the results of the performed independent temperature test checks mapped on SDN L20
856 vocabulary;
- 857 • *TEMPET01_INT_SEADATANET_QC*: it contains flags associated with the temperature interpolated
858 profile.

859

860 **C.5 Additional variables**

861 In addition to attributes, some variables from the SDN extension have been adopted:

- 862 1. *SDN_CRUISE*: an array containing the name of project which funded the cruise;
- 863 2. *SDN_EDMO_CODE*: an integer array containing keys identifying the organization in the European
864 Directory of Marine Organizations (EDMO, <https://www.seadatanet.org/Metadata/EDMO-Organisations>)
865
- 866 3. *SDN_BOT_DEPTH*: a floating point array holding bathymetric water depth in meters where the
867 sample was collected or measurement was made. We considered the local bottom depth extracted from
868 the GEBCO Compilation Group (2021).

869

870 Moreover, in order to preserve and keep track of metadata associated with each profile in the dissemination
871 through ERDDAP, other variables have been adopted:

- 872 4. *cruise_id*: an array containing the name of the project which funded the cruise plus the year and the
873 month of the cruise;
- 874 5. *profile_id*: an array referring to the sequence of the profile during the corresponding cruise.

875 **C.6 Global metadata fields**

876 The global attribute section of the NetCDF file describes its content overall. All attributes should be human-
877 readable and contain meaningful information for data discovery and re-use. Most importantly, all available
878 discovery metadata to the SDN mandatory attributes have been introduced following recommendations of the
879 XBT community. Moreover, several studies (Cheng et al., 2014; 2016; 2018; Goni et al., 2019) highlighted
880 the dependency of the biases on probe type, time (due to variations in the manufacturing process) and changes
881 in the recording systems (Tan et al., 2021). For these reasons, the following information has been inserted in
882 the XBT metadata description: probe type with serial number, manufacturer, manufacturing date, FRE
883 coefficients used to calculate the depth, launch height, DAQ model and recorder version (Cheng et al., 2016).
884 Ship speed, wind speed, and probe mass (available since 2018) have been added to this metadata section. When
885 available, mass of the XBT probe, wind speed and ship speed are other useful information included in this
886 metadata section.



887 The above mentioned information has been kept and made available through the ERDDAP by an `url_metadata`
888 variable associated to the entire dataset, which contains details specific to each profile.
889



890 **References**

- 891 Anderson, E.A.: Expendable bathythermograph (XBT) accuracy studies, Tech. Rep. 550, Naval Ocean System
892 Center, California, 201 pp, June 1980. <https://doi.org/10.5962/bhl.title.47513>, 1980.
- 893 Bailey, R., Gronell A., Phillips H., Tanner E. and Meyers G.: Quality Control Cookbook for XBT Data. CSIRO
894 Report 221, 84 pp, 1994. <http://hdl.handle.net/102.100.100/237126?index=1>
- 895 Barker, P.M., and McDougall, T.J.: Two Interpolation Methods Using Multiply-Rotated Piecewise Cubic
896 Hermite Interpolating Polynomials. *J. Atmos. Oceanic Technol.*, 37(4), 605–619.
897 <https://doi.org/10.1175/JTECH-D-19-0211.1>, 2020.
- 898 Bordone, A., Pennechi F., Raiteri G., Repetti L., Reseghetti F.: XBT, ARGO Float and Ship-Based CTD
899 Profiles Intercompared under Strict Space-Time Conditions in the Mediterranean Sea: Assessment of
900 Metrological Comparability. *Journal of Marine Science and Engineering*, 8(5):313.
901 <https://doi.org/10.3390/jmse8050313>, 2020.
- 902 Bringas, F., and Goni, G.: Early dynamics of Deep Blue XBT probes, *J. Atmos. Oceanic Technol.*, 32(12),
903 2253–2263. <https://doi.org/10.1175/JTECH-D-15-0048.1>, 2015.
- 904 Chen, C.: Evaluation of resistance–temperature calibration equations for NTC thermistors. *Measurement*, 42,
905 1103–1111, doi:10.1016/j.measurement.2009.04.004.
- 906 Cheng, L., Abraham, J., Trenberth, K.E. et al. Another Record: Ocean Warming Continues through 2021
907 despite La Niña Conditions. *Adv. Atmos. Sci.* 39, 373–385 (2022). [https://doi.org/10.1007/s00376-022-1461-](https://doi.org/10.1007/s00376-022-1461-3)
908 [3](https://doi.org/10.1007/s00376-022-1461-3)
- 909 Cheng, L., Abraham, J., Trenberth, K.E. et al. Upper Ocean Temperatures Hit Record High in 2020. *Adv.*
910 *Atmos. Sci.* 38, 523–530 (2021). <https://doi.org/10.1007/s00376-021-0447-x>
- 911 Cheng, L., Abraham, J., Zhu, J. et al. Record-Setting Ocean Warmth Continued in 2019. *Adv. Atmos. Sci.* 37,
912 137–142 (2020). <https://doi.org/10.1007/s00376-020-9283-7>
- 913 Cheng, L., and Coauthors: How well can we correct systematic errors in historical XBT data? *J. Atmos.*
914 *Oceanic Technol.*, 35, 1103–1125, doi:10.1175/jtech-d-17-0122.1, 2018.
- 915 Cheng, L., et al., Improved estimates of ocean heat content from 1960 to 2015. *Sci. Adv.* 3, e1601545 (2017).
916 DOI:10.1126/sciadv.1601545
- 917 Cheng, L., and Coauthors: XBT science: assessment of instrumental biases and errors. *Bull. Amer. Meteor.*
918 *Soc.* 97, 923–934, doi:10.1175/Bams-D-15-00031.1, 2016.
- 919 Cheng, L., J. Zhu, R. Cowley, T. Boyer, and S. Wijffels: Time, probe type, and temperature variable bias
920 corrections to historical expendable bathythermograph observations. *J. Atmos. Oceanic Technol.*, 31, 1793–
921 1825, doi:10.1175/Jtech-D-13-00197.1, 2014.
- 922
- 923 Cook, S. and Sy A.: Best guide and principles manual for the Ships Of Opportunity Program (SOOP) and
924 eXpendable BathyThermograph (XBT) operations, Geneva, Switzerland, WMO & IOC, 26pp. DOI:
925 <https://doi.org/10.25607/OBP-1483>.
- 926 Cowley R., Killick R.E., Boyer T., Gouretski V., Reseghetti F., Kizu S., Palmer M.D., Cheng L., Storto A., Le
927 Menn M., Simoncelli S., Macdonald A.M. and Domingues C.M.: International Quality-Controlled Ocean
928 Database (IQOD) v0.1: The Temperature Uncertainty Specification. *Front. Mar. Sci.* 8:689695. doi:
929 10.3389/fmars.2021.689695, 2021.



- 930 Cowley, R., and Krummel, L.: Australian XBT Quality Control Cookbook Version 2.0. Report EP2022-1825
931 CSIRO, Australia, pp. 1-89 <https://doi.org/10.25919/3tm5-zn80>, 2022.
- 932 Durante S, Oliveri P, Nair R and Sparnocchia S (2021) Mixing in the Tyrrhenian Interior Due to Thermohaline
933 Staircases. *Front. Mar. Sci.* 8:672437. doi: 10.3389/fmars.2021.672437
- 934 Flierl, G. R., and A. R. Robinson, 1977: XBT Measurements of Thermal Gradients in the MODE Eddy. *J.*
935 *Phys. Oceanogr.*, 7, 300–302, [https://doi.org/10.1175/1520-0485\(1977\)007<0300:XMOTGI>2.0.CO;2](https://doi.org/10.1175/1520-0485(1977)007<0300:XMOTGI>2.0.CO;2).
- 936 Fusco, G., Manzella, G. M. R., Cruzado, A., Gacic, M., Gasparini, G. P., Kovacevic, V., Millot, C., Tziavos,
937 C., Velasquez, Z., Walne, A., Zervakis, V., and Zodiatis, G.: Variability of mesoscale features in the
938 Mediterranean Sea from XBT data analysis, *Ann. Geophys.*, 21, 21–32, [http://www.ann-](http://www.ann-geophys.net/21/21/2003/)
939 [geophys.net/21/21/2003/](http://www.ann-geophys.net/21/21/2003/), 2003.
- 940 GEBCO Compilation Group: GEBCO 2021 Grid. doi:10.5285/c6612cbe-50b3-0cff-e053-6c86abc09f8f,
941 2021.
- 942 Goni, G., and Coauthors: More than 50 years of successful continuous temperature section measurements by
943 the global expendable bathythermograph network, its integrability, societal benefits, and future. *Front. Mar.*
944 *Sci.*, 6:452, doi:10.3389/fmars.2019.00452, 2019.
- 945 Haddad, S., R. E. Killick, M. D. Palmer, M. J. Webb, R. Prudden, F. Capponi, and S. V. Adams, 2022:
946 Improved Infilling of Missing Metadata from Expendable Bathythermographs (XBTs) Using Multiple
947 Machine Learning Methods. *J. Atmos. Oceanic Technol.*, 39, 1367–1385, [https://doi.org/10.1175/JTECH-D-](https://doi.org/10.1175/JTECH-D-21-0117.1)
948 [21-0117.1](https://doi.org/10.1175/JTECH-D-21-0117.1).
- 949 Hanawa, K., P. Rual, R. Bailey, A. Sy, and M. Szabados: A new depth-time equation for Sippican or TSK T-
950 7, T-6 and T-4 expendable bathythermographs (XBT). *Deep-Sea Res. I*, 42, 1423–1451, doi:10.1016/0967-
951 0637(95)97154-Z, 1995.
- 952 Hoge, H.: Useful procedure in least squares, and tests of some equations for thermistors. *Rev. Sci. Instrum.*,
953 59, 975-979, doi:10.1063/1.1139762, 1988.
- 954 Intergovernmental Oceanographic Commission (2013) Ocean Data Standards Volume 3. Recommendation for
955 a Quality Flag Scheme for the Exchange of Oceanographic and Marine Meteorological Data. Paris, France,
956 UNESCO-IOC, 5pp. & Annexes. (Intergovernmental Oceanographic Commission Manuals and Guides,
957 Volume 54 (3). (IOC/2013/MG/54-3) <http://dx.doi.org/10.25607/OBP-6>.
- 958 Intergovernmental Oceanographic Commission (2019) Ocean Data Standards Volume 4: Technology for
959 SeaDataNet Controlled Vocabularies for describing Marine and Oceanographic Datasets - A joint Proposal by
960 SeaDataNet and ODIP projects. Oostend, Belgium, IODE/UNESCO, 31pp. (IOC Manuals and Guides, 54,
961 Vol. 4. Version 1), (IOC/2019/MG/54 Vol.4). DOI: <http://dx.doi.org/10.25607/OBP-566>
- 962 Leahy, T. P., F. P. Llopis, M. D. Palmer, and N. H. Robinson, 2018: Using Neural Networks to Correct
963 Historical Climate Observations. *J. Atmos. Oceanic Technol.*, 35, 2053–2059, [https://doi.org/10.1175/JTECH-](https://doi.org/10.1175/JTECH-D-18-0012.1)
964 [D-18-0012.1](https://doi.org/10.1175/JTECH-D-18-0012.1).
- 965 Li, Y., Church, J. A., McDougall, T.J., and Barker, P. M.: Sensitivity of observationally based estimates of
966 ocean heat content and thermal expansion to vertical interpolation schemes. *Geophysical Research Letters*, 49,
967 e2022GL101079. <https://doi.org/10.1029/2022GL101079>, 2022.
- 968 Liu, G., L. Guo, C. Liu, and Q. Wu: Evaluation of different calibration equations for NTC thermistor applied
969 to high-precision temperature measurement. *Measurement*, 120, 21-27,
970 doi:10.1016/j.measurement.2018.02.007, 2018.



- 971 Lowry, R.; Fichaut, M. and Bregent S.: SeaDataNet NetCDF format definition. Version 1.21. SeaDataNet,
972 73pp. DOI: <http://dx.doi.org/10.25607/OBP-408>, 2019.
- 973 Manzella, G. M. R., Scoccimarro, E., Pinardi, N., and Tonani, M.: "Improved near real time data management
974 procedures for the Mediterranean ocean Forecasting System – Voluntary Observing Ship Program", *Ann.*
975 *Geophys.*, 21, pp. 49–62. <https://doi.org/10.5194/angeo-21-49-2003>, 2003.
- 976 Manzella, G. M. R., Reseghetti, F., Coppini, G., Borghini, M., Cruzado, A., Galli, C., Gertman, I., Gervais, T.,
977 Hayes, D., Millot, C., Murashkovsky, A., Özsoy, E., Tziavos, C., Velasquez, Z., and Zodiatis, G.: The
978 improvements of the ships of opportunity program in MFS-TEP, *Ocean Sci.*, 3, 245–258,
979 <https://doi.org/10.5194/os-3-245-2007>, 2007.
- 980 Meccia, V. L., Simoncelli, S., & Sparnocchia, S. (2016). Decadal variability of the Turner Angle in the
981 Mediterranean Sea and its implications for double diffusion. *Deep Sea Research Part I: Oceanographic*
982 *Research Papers*, 114, 64–77. <https://doi.org/10.1016/J.DSR.2016.04.001>
- 983 Meyssignac B., Boyer T., Zhao Z., et al.: Measuring Global Ocean Heat Content to Estimate the Earth Energy
984 Imbalance. *Front. Mar. Sci.* 6:432. <https://doi.org/10.3389/fmars.2019.00432>, 2019.
- 985 Millot, C., Taupier-Letage, I. (2005a). Circulation in the Mediterranean Sea. In: Saliot, A. (eds) *The*
986 *Mediterranean Sea. Handbook of Environmental Chemistry*, vol 5K. Springer, Berlin, Heidelberg.
987 <https://doi.org/10.1007/b107143>
- 988 Millot, C. and Taupier-Letage, I., 2005b: Additional evidence of LIW entrainment across the Algerian Basin
989 by mesoscale eddies and not by permanent westward-flowing vein, *Progress in Oceanography*, 231–250.
990 <https://doi.org/10.1016/j.pocean.2004.03.002>
- 991 OceanSITES, 2020: OceanSITES Data Format Reference Manual NetCDF Conventions and Reference Tables.
992 Version 1.4 July 16, 2020. Geneva, Switzerland, OceanSITES, JCOMMOPS, 36pp. DOI:
993 <http://dx.doi.org/10.25607/OBP-421.2>
- 994 Palmer, M. D., T. Boyer, R. Cowley, S. Kizu, F. Reseghetti, T. Suzuki, and A. Thresher, 2018: An Algorithm
995 for Classifying Unknown Expendable Bathythermograph (XBT) Instruments Based on Existing Metadata. *J.*
996 *Atmos. Oceanic Technol.*, 35, 429–440, <https://doi.org/10.1175/JTECH-D-17-0129.1>.
- 997 Parks, J., Bringas, F., Cowley, R., Hanstein, C., Krummel, L., Sprintall, J., Cheng, L., Cirano, M., Cruz, S.,
998 Goes, M., Kizu, S. and Reseghetti, F., 2022: XBT operational best practices for quality assurance. *Front. Mar.*
999 *Sci.* 9:991760. doi: 10.3389/fmars.2022.991760
- 1000 Pinardi, N., Allen, I., Demirov, E., De Mey, P., Korres, G., Lascaratos, A., Le Traon, P.-Y., Maillard, C.,
1001 Manzella, G., and Tziavos, C., 2003: The Mediterranean ocean forecasting system: first phase of
1002 implementation (1998–2001), *Ann. Geophys.*, 21, 3–20, <https://doi.org/10.5194/angeo-21-3-2003>
- 1003 Pinardi, N., and Coppini, G., 2010: Preface" Operational oceanography in the Mediterranean Sea: the second
1004 stage of development". *Ocean Science*, 6(1), 263-267, <https://doi.org/10.5194/os-6-263-2010>, 2010.
- 1005 Pinardi N, Stander J, Legler DM, O'Brien K, Boyer T, Cuff T, Bahurel P, Belbeoch M, Belov S, Brunner S,
1006 Burger E, Carval T, Chang-Seng D, Charpentier E, Ciliberti S, Coppini G, Fischer A, Freeman E, Gallage C,
1007 Garcia H, Gates L, Gong Z, Hermes J, Heslop E, Grimes S, Hill K, Horsburgh K, Iona A, Mancini S, Moodie
1008 N, Ouellet M, Pissierssens P, Poli P, Proctor R, Smith N, Sun C, Swail V, Turton J and Xinyang Y (2019) The
1009 Joint IOC (of UNESCO) and WMO Collaborative Effort for Met-Ocean Services. *Front. Mar. Sci.* 6:410. doi:
1010 10.3389/fmars.2019.00410
- 1011 Plessey Company Limited, 1975: Plessey-Sippican expendable bathythermograph system, Tech. Rep.
1012 MP0400, Issue 0401, January 1975, 51 pp.



- 1013 R.F. Reiniger, C.K. Ross, 1968: A method of interpolation with application to oceanographic data, *Deep Sea*
1014 *Research and Oceanographic Abstracts*, Volume 15, Issue 2, Pages 185-193, ISSN 0011-7471,
1015 [https://doi.org/10.1016/0011-7471\(68\)90040-5](https://doi.org/10.1016/0011-7471(68)90040-5).
- 1016 Reseghetti, F., M. Borghini, and G. M. R. Manzella, 2007: Factors affecting the quality of XBT data—Results
1017 of analyses on profiles from the Western Mediterranean Sea. *Ocean Science*, 3, 59–75,
1018 <https://doi.org/10.5194/os-3-59-2007>
- 1019 Reseghetti, F., L. Cheng, M. Borghini, I. M. Yashayaev, G. Raiteri, and J. Zhu, 2018: Assessment of Quality
1020 and Reliability of Measurements with XBT Sippican T5 and T5/20. *J. Atmos. Oceanic Technol.*, 35, 1935–
1021 1960, <https://doi.org/10.1175/JTECH-D-18-0043.1>.
- 1022 Reseghetti F., Fratianni C., Simoncelli S. (2023). Reprocessed of XBT dataset in the Ligurian and Tyrrhenian
1023 seas (1999-2019). Istituto Nazionale di Geofisica e Vulcanologia (INGV).
1024 https://doi.org/10.13127/rep_xbt_1999_2019
- 1025 Simoncelli, S., Schaap, D., Schlitzer, R., 2020a: Mediterranean Sea - Temperature and salinity Historical Data
1026 Collection SeaDataCloud V2. <https://doi.org/10.12770/2a2aa0c5-4054-4a62-a18b-3835b304fe64>
- 1027 Simoncelli, S., Oliveri, P., Mattia, G., Myroshnychenko, V., 2020b: SeaDataCloud Temperature and Salinity
1028 Historical Data Collection for the Mediterranean Sea (Version 2). Product Information Document (PIDoc).
1029 <https://doi.org/10.13155/77059>
- 1030 S. Simoncelli, G. M.R. Manzella, A. Storto, A. Pisano, M. Lipizer, A. Barth, V. Myroshnychenko, T. Boyer,
1031 C. Troupin, C. Coatanoan, A. Pititto, R. Schlitzer, Dick M.A. Schaap, S. Diggs, Chapter Four - A collaborative
1032 framework among data producers, managers, and users, Editor(s): Giuseppe Manzella, Antonio Novellino,
1033 *Ocean Science Data*, Elsevier, 2022, Pages 197-280, ISBN 9780128234273, [https://doi.org/10.1016/B978-0-](https://doi.org/10.1016/B978-0-12-823427-3.00001-3)
1034 [12-823427-3.00001-3](https://doi.org/10.1016/B978-0-12-823427-3.00001-3)
- 1035 Sippican Corp.: Instructions for installation, operation and maintenance of Sippican expendable
1036 bathythermograph system - M300, R-467B, 100 pp, 1968.
- 1037 Sippican: Instruction manual for the expendable bathythermograph system, R-603G - 1971, Sept. 1980. The
1038 Sippican Corporation Ocean Systems Division, 208 pp, 1980.
- 1039 Sippican, Inc.: Sippican MK12 oceanographic data acquisition system user's manual, Sippican, Inc., User's
1040 Manual R-2626/B P/N 306130-1, August 1991, 166 pp., 1991.
- 1041 Lockheed Martin Sippican (Sippican) Inc.: MK21 USB DAQ, surface ship, bathythermograph data acquisition
1042 system, installation operation and maintenance manual, P/N 308437, Rev. E, 172 pp, 2006.
- 1043 Lockheed Martin Sippican (Sippican) Inc.: WinMK21 Data Acquisition and Post Processing Software User's
1044 Manual P/N 352210, Rev. B, 134 pp, 2010.
- 1045 Lockheed Martin Sippican (Sippican) Inc.: MK21 Ethernet Surface 1U DAQ - Bathythermograph data
1046 acquisition system, installation and operation manual, P/N 352186, Rev. D, 47 pp, 2014.
- 1047 Sy, A.: XBT Measurements. In: WOCE Operations Manual, Part 3.1.3 WHP Operations and Methods, WHP
1048 Office Report, WHPO 91-1, 19 pp., 1991.
- 1049 Sy, A., and D. Wright: XBT/XCTD standard test procedures for reliability and performance test of expendable
1050 probes at sea. Revised draft. Geneva, Switzerland, WMO, TC SOT JCOMM Ship Observations Team, 8pp.
1051 DOI: <https://doi.org/10.25607/OBP-1487>
- 1052 Tan, Z., Reseghetti, F., Abraham, J., Cowley, R., Chen, K., Zhu, J., Zhang, B., and Cheng, L.: Examining the
1053 Influence of Recording System on the Pure Temperature Error in XBT Data. *J. Atmos. Oceanic Technol.*
1054 doi:10.1175/JTECH-D-20-0136.1, 2021.



- 1055 Tanhua T, Pouliquen S, Hausman J, O'Brien K, Bricher P, de Bruin T, Buck JJH, Burger EF, Carval T, Casey
1056 KS, Diggs S, Giorgetti A, Glaves H, Harscoat V, Kinkade D, Muelbert JH, Novellino A, Pfeil B, Pulsifer PL,
1057 Van de Putte A, Robinson E, Schaap D, Smirnov A, Smith N, Snowden D, Spears T, Stall S, Tacoma M,
1058 Thijsse P, Tronstad S, Vandenberghe T, Wengren M, Wyborn L and Zhao Z (2019) Ocean FAIR Data Services.
1059 *Front. Mar. Sci.* 6:440. doi: 10.3389/fmars.2019.00440
- 1060 Vignudelli, S., Cipollini, P., Reseghetti, F., Fusco, G., Gasparini, G.P., Manzella, G.M.R.: Comparison
1061 between XBT data and TOPEX/Poseidon satellite altimetry in the Ligurian-Tyrrhenian area, *Annales*
1062 *Geophysicae*, 21, 123-135, doi:10.5194/angeo-21-123-2003, 2003.
- 1063 K von Schuckmann, P-Y Le Traon, E Alvarez-Fanjul, L Axell, M Balmaseda, L-A Breivik, R J. W. Brewin,
1064 C Bricaud, M Drevillon, Y Drillet, C Dubois, O Embury, H Etienne, M Garcia Sotillo, G Garric, F Gasparin,
1065 E Gutknecht, S Guinehut, F Hernandez, M Juza, B Karlson, G Korres, J-F Legeais, B Levier, V S. Lien, R
1066 Morrow, G Notarstefano, L Parent, Á Pascual, B Pérez- Gómez, C Perruche, N Pinardi, A Pisano, P-M Poulain,
1067 I M. Pujol, R P. Raj, U Raudsepp, H Roquet, A Samuelsen, S Sathyendranath, J She, S Simoncelli, C Solidoro,
1068 J Tinker, J Tintoré, L Viktorsson, M Ablain, E Almroth-Rosell, A Bonaduce, E Clementi, G Cossarini, Q
1069 Dagneaux, C Desportes, S Dye, C Fratianni, S Good, E Greiner, J Gourrion, M Hamon, J Holt, P Hyder, J
1070 Kennedy, F Manzano- Muñoz, A Melet, B Meyssignac, S Mulet, B Buongiorno Nardelli, E O'Dea, E Olason,
1071 A Paulmier, I Pérez-González, R Reid, M-F Racault, D E. Raitsos, A Ramos, P Sykes, T Szekely & N
1072 Verbrugge (2016) The Copernicus Marine Environment Monitoring Service Ocean State Report, *Journal of*
1073 *Operational Oceanography*, 9:sup2, s235-s320, <http://dx.doi.org/10.1080/1755876X.2016.1273446>
- 1074 Wilkinson, M., Dumontier, M., Aalbersberg, I. et al. The FAIR Guiding Principles for scientific data
1075 management and stewardship. *Sci Data* 3, 160018 (2016). <https://doi.org/10.1038/sdata.2016.18>
- 1076 Zodiatis, G., Drakopoulos, P., Brenner, S., & Groom, S. 2005. Variability of the Cyprus warm core Eddy
1077 during the CYCLOPS project. *Deep Sea Research Part II: Topical Studies in Oceanography*, 52(22-23), 2897–
1078 2910. <https://doi.org/10.1016/j.dsr2.2005.08.020>